LLE Review
Quarterly Report

September, 1980 – December, 1980

UR
LLE

LLE Review

Quarterly Report

Editor: John A. Boles
(716-275-2315)

September, 1980 – December, 1980

UR
LLE

IN BRIEF

The month of December has been included in this issue of the LLE Review to adjust the publication schedule to coincide with calendar quarters. This period from September through December, 1980 was highlighted by single beam ultraviolet target absorption experiments. These initial experiments, carried out using the GDL laser system, have shown target absorption fractions two to three times those in the infrared. Additional achievements include:

- Large aperture liquid crystal optical isolators demonstrated contrast ratios greater that 130:1 with damage thresholds greater than 2 J/cm².

- Studies in the nonlinear evolution of the Raleigh - Taylor instability indicate that targets may be designed with higher aspect ratios than linear theory would have predicted.

- Zone plates for coded imaging of hard x-rays have been produced with thicknesses of 40 μm and outer zone widths of 10 μm.

- A new technique has been developed to produce laser pulses shorter than 2 psec by synchronously pumping a Rhodamine 6G dye laser.

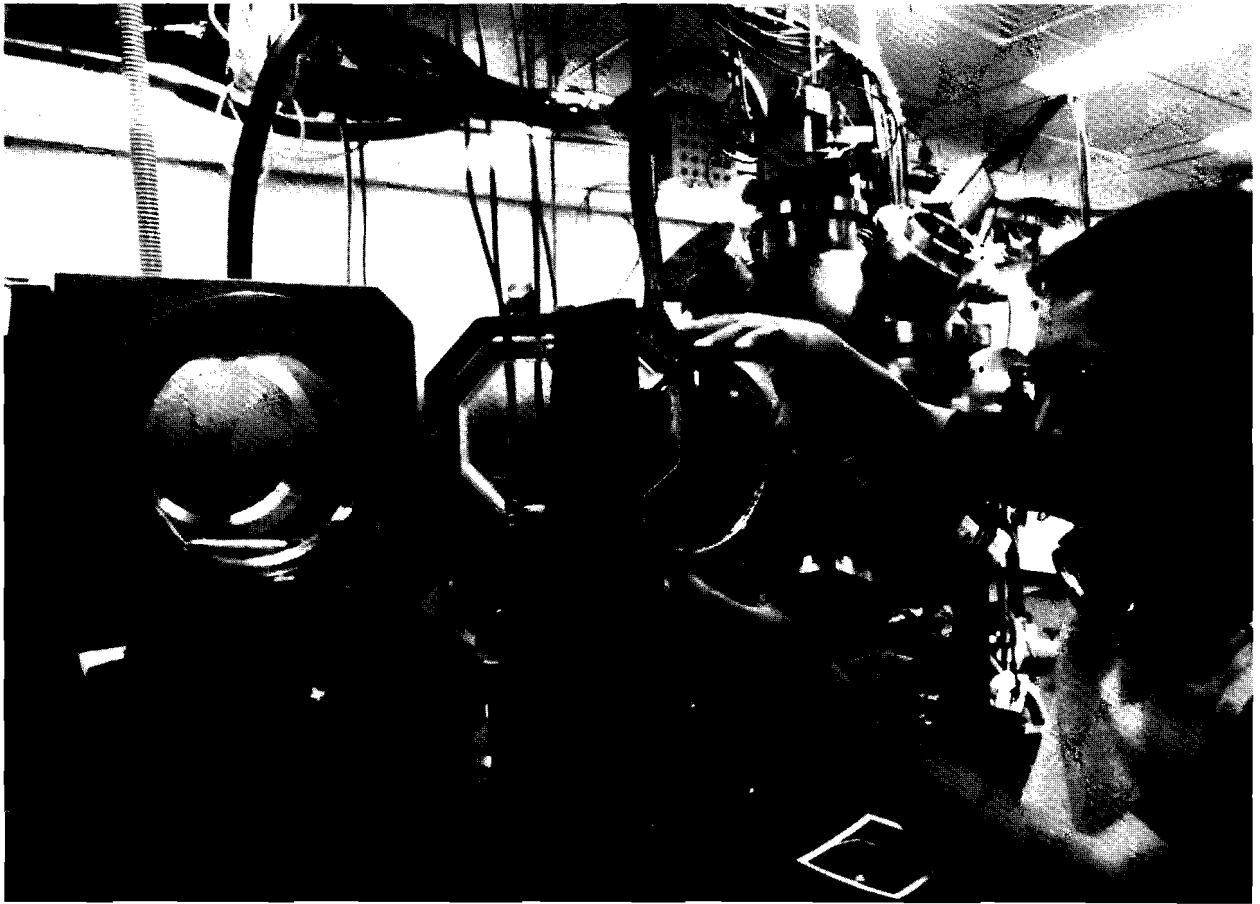Each of these achievements is described in this volume of the LLE Review.

On January 22, Dr. Moshe J. Lubin resigned from his position as Director of the Laboratory for Laser Energetics, a position held since 1970. Dr. Lubin has taken a position with the Standard Oil

Company (Ohio) as Vice President of Research, Development, Patents, and Licenses.

Dr. Jay M. Eastman succeeds Dr. Lubin as Acting Director of the Laboratory for Laser Energetics. Dr. Eastman previously served as the Deputy Director of the Laboratory and as the Director of the Division of Engineering.

CONTENTS

Kazuo Tanaka adjusting a collimating lens for the ultraviolet alignment beam in the GDL target area. The pulsed beam and alignment beam are combined at this point on a beam splitter prior to the tripling crystals. The GDL target chamber appears in the background where absorption and laser plasma interaction experiments are being conducted in the ultraviolet.

Section 1
LASER SYSTEM REPORT

1.A OMEGA Facility Report

Initial steps were undertaken at LLE to characterize the uniformity of illumination on the target surface. The theoretical modeling of target illumination as well as preliminary beam propagation tests were reported in Volume 4 of the LLE Review. During this quarter the OMEGA laser system was used to provide laser system code normalization data as well as study the pointing and focusing of the laser on laser fusion targets.

The pointing and focusing of OMEGA beams was studied by photographing the x-ray emission of targets irradiated by two or six OMEGA beams. Several target shots studying these effects were taken during this period. The x-ray photographs were digitized and compared with an expected x-ray emission distribution. Figure 1(c) shows a result of a six beam shot on an empty glass microballoon 231 μm in diameter with 2.5 μm wall thickness. The laser was operated with a pulse width of 257 psec and an energy of 228 J on target. Figure 1(a) shows the six beam geometry as viewed by the x-ray pinhole camera; Fig. 1(b) shows the x-ray contours of constant intensity calculated from the photograph in Fig. 1(c). This result shows the OMEGA beams to be pointed to better than 8 μrad on target. This has provided initial verification of the ability to conduct target experiments on OMEGA with a high degree of confidence in the system alignment. More extensive calibration shots will be performed on OMEGA during the next quarter.
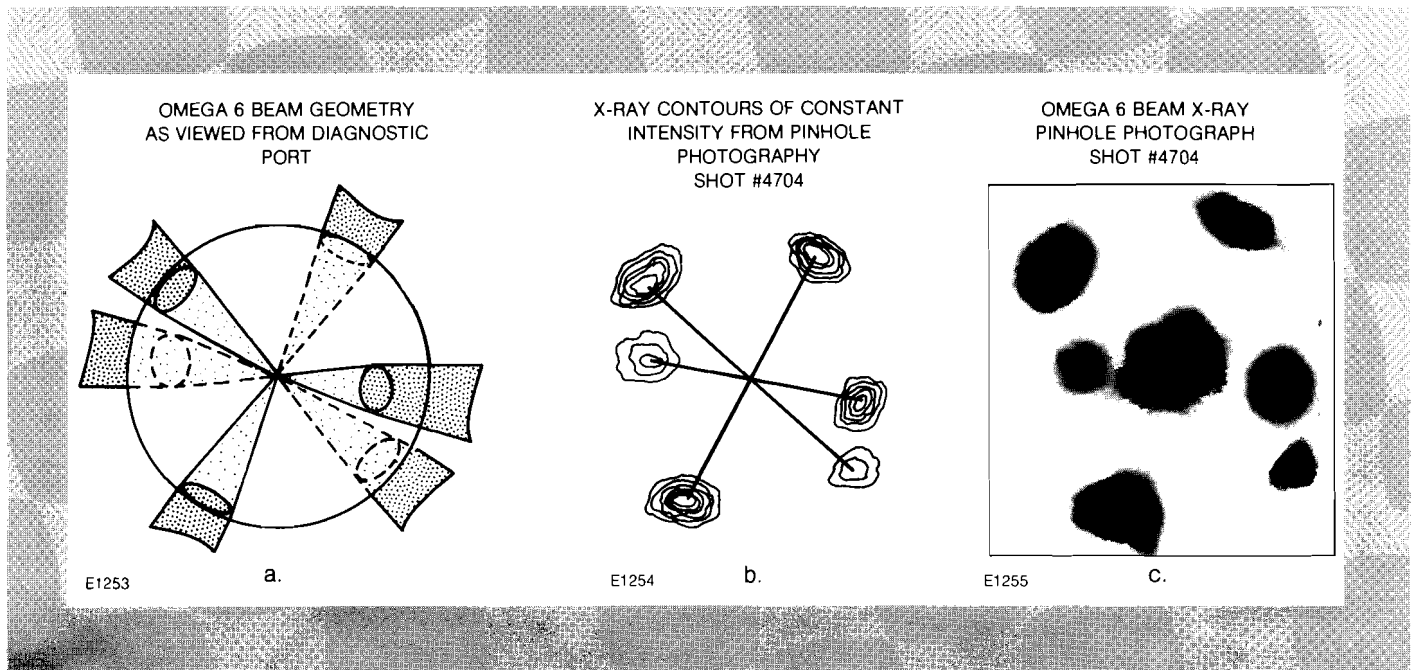
OMEGA 6 BEAM GEOMETRY
AS VIEWED FROM DIAGNOSTIC
PORT

X-RAY CONTOURS OF CONSTANT
INTENSITY FROM PINHOLE
PHOTOGRAPHY
SHOT #4704

OMEGA 6 BEAM X-RAY
PINHOLE PHOTOGRAPH
SHOT #4704

E1253   a.

E1254   b.

E1255   c.

Fig. 1
The geometry of irradiation on the surface of an OMEGA target as viewed from the pinhole camera diagnostic port (a), a sample x-ray pinhole photograph (c), and a plot of equal intensity contours from the pinhole photograph (b), show that the OMEGA laser beams are pointed to better than 8 μrad.

A program was formulated this quarter to further pursue the evaluation of the present performance of OMEGA to provide an understanding of the intensity profile on-target and to allow normalization of several propagation codes.

The first four laser amplifiers in the OMEGA system (called the driverline) are the most critical for affecting the laser output spatial intensity profile because of the large magnification (60X), the high gain (4 $\times$ 10⁶) and the nonuniform radial gain profiles. These four laser amplifiers were removed from the system and their small signal radial gain profiles were measured to improve our existing data, which was for a different laser glass composition and neodymium doping. The details of the measurements are reported in LLE Report #110. This data will be used to model the performance of this important section of the laser. This capability will allow us to evaluate various driverline configurations in order to optimize the output intensity profile of OMEGA.

Near field photos were taken at the locations shown in Fig. 2 to provide additional data for normalizing the propagation codes. Digitization and processing of these images will proceed through the next quarter. Each piece of film was individually calibrated with a series of spots which vary by a known intensity ratio. This will allow accurate calculation of the beam intensity from the photo density. These photos were taken with a pulse width of 600 psec. Additional short pulse photos will be taken in the future.

Additional testing of the quality of an OMEGA beam at the target will be conducted in the next quarter.

The Laboratory for Laser Energetics is proceeding on a program to do direct-driven implosions at short wavelength (around 350 nm) on OMEGA. These experiments require nanosecond pulse widths,

so a second oscillator was brought on-line on OMEGA to produce pulses of 600-700 psec. This oscillator, and the existing short pulse oscillator, provide OMEGA with the flexibility to operate at the 100 psec and 700 psec regimes with a minimal change-over time. This longer pulse oscillator is an active-passive cavity similar to the short pulse oscillator which has been running on OMEGA for several years.[1] A more flexible oscillator similar to the Kuizenga oscillator of LLNL[2] will be put on-line on OMEGA during the third or fourth quarter.

REFERENCES

1. W. Seka, J. Bunkenburg, "Active-Passive Mode-Locked Oscillators at 1.054 μm," *J. Appl. Phys.* **49** 2277 (1978).

2. A.E. Siegman, D.J. Kuizenga, *Opto Electronics* **6**, 43-66 (1974).
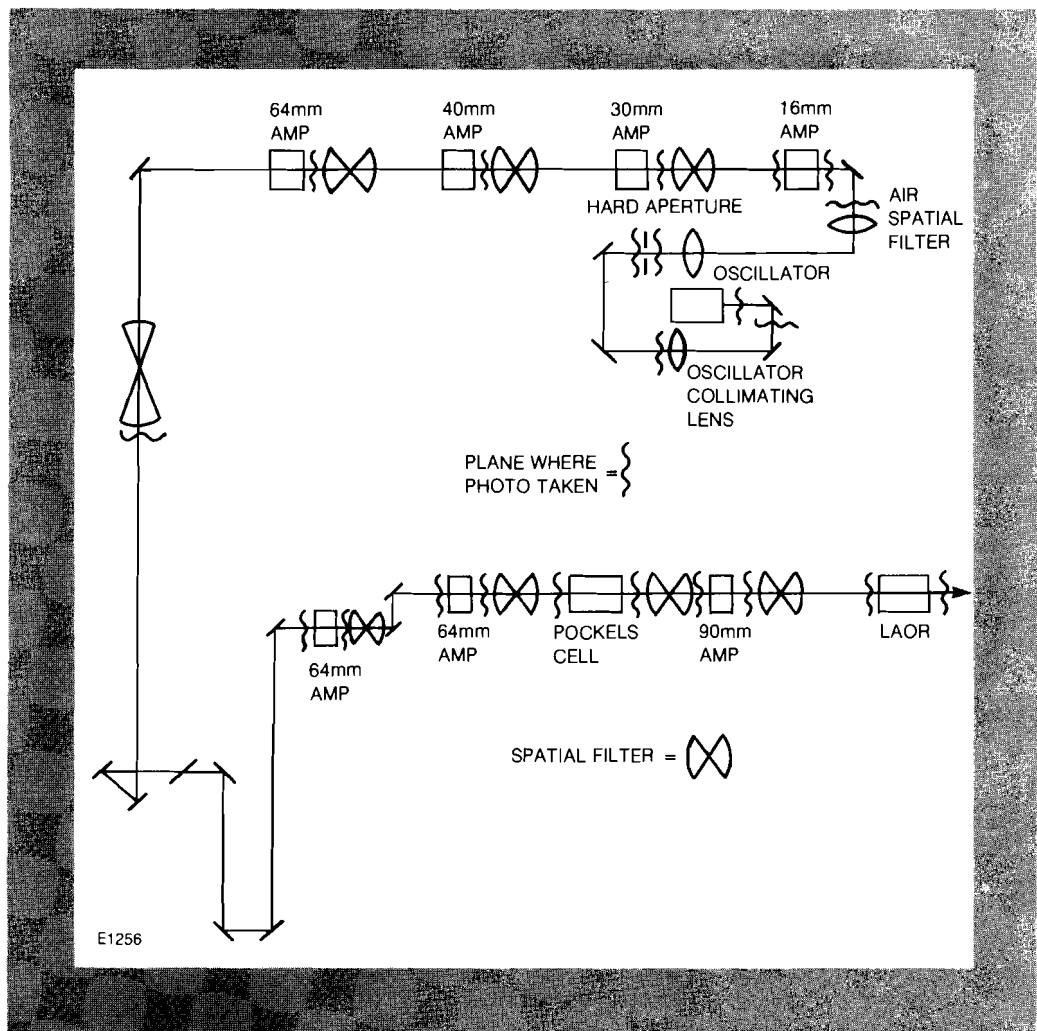
Fig. 2
Near field photograph locations for propagation code normalization. Comparison of actual intensity distribution are made with calculated intensity distribution at these locations.

1.B GDL Facility Report

During the first quarter of FY 1981, GDL began operations as a 0.35 μm irradiation facility. The basis of this facility is the Glass Development Laser system originally constructed as a prototype of an OMEGA beam line.[1] With the addition of frequency conversion crystals, ultraviolet optics and an ultraviolet alignment and beam diagnostics system, the facility is now one of the most powerful ultraviolet irradiation systems in the world. The current capabilities of the GDL 0.35 μm facility are listed in Table 1. Later in the year the capabilities of this system will be enhanced with the addition of faster optics (f/3) and crystals optimized for longer pulse operation.

Table 1
Current capabilities of GDL, 0.35 μm irradiation facility.

ON TARGET POWER:	200 GW (100 psec) @ 0.35 μm
ON TARGET ENERGY:	50J (450 psec) @ 0.35 μm
	25J (100 psec) @ 0.35 μm
ON TARGET INTENSITY:	10^{12} to 5×10^{15} W/cm^2
FOCUSING OPTICS:	f/12 Quartz Lens
SPOT SIZE:	80 - 800 μm Diameter
FUNDAMENTAL AND SECOND HARMONIC SUPPRESSION:	10^4 in Intensity
	10^2 in Energy

E1257

The design of the frequency conversion system used on the GDL 0.35 μm irradiation facility was based on the development work conducted on GDL in 1980.[2,3] Design details of the system are presented elsewhere in this report. During the first quarter of FY 81, the system was operated in short pulse mode (100 psec FWHM at 0.35 μm) for frequency conversion tests, coating damage tests, and initial interaction experiments.

The facility delivered a total of 409 shots during this time. The shot distribution was as follows:

3ω Conversion Tests	171 Shots
3ω Diagnostics C/O	63
3ω Target Experiments	48
Damage Test Facility	106
Beam Alignment	11
Failed Shots	10
TOTAL	409 Shots

Figure 3 illustrated the excellent stability of both the GDL driver and the frequency conversion system.

REFERENCES
1. W. Seka, J. Soures, O. Lewis, J. Bunkenburg, D. Brown, S.

Jacobs, G. Mourou, and J. Zimmerman, *Appl. Optics* **19**, 409 (1980).

2.   W. Seka, S. D. Jacobs, J. E. Rizzo, R. Boni and R. S. Craxton, *Opt. Comm.* **34**, 469 (1980).

3.   R. S. Craxton, *Opt. Comm.* **34**, 474 (1980).

Fig. 3
GDL 0.35 μm irradiation facility performance on 0.35μm target shots during the period 3-20 November, 1980. The solid lines shows the 1.054 μm energy requested by the experimentalists, the filled dots show the actual 1.054 μm energy delivered to the conversion crystals and the open dots show the 0.35 μm energy delivered to the target. All of the shots were at a pulse width of 100 psec at 0.35 μm.
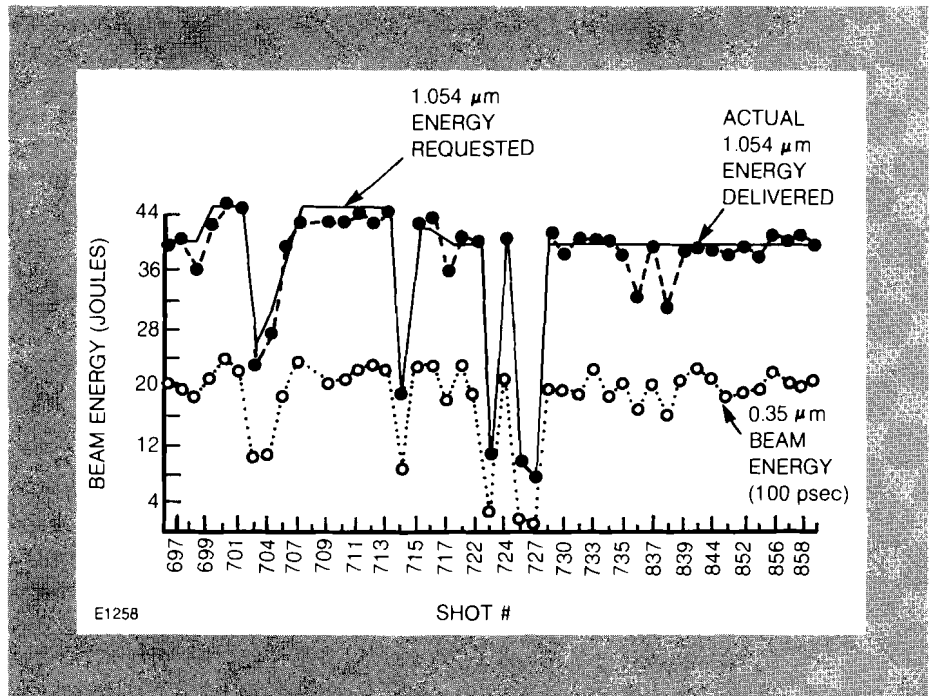
1.C Liquid Crystal Devices for High Power Lasers – Part I: Optical Isolators

Liquid crystals constitute a unique state of matter. They can flow over surfaces as easily as liquids, and yet they possess a long range structural order characteristic of crystalline solids. Liquid crystal compounds are not rare. Over 20,000 compounds have been found or synthesized since their discovery in 1888.[1,2] These substances have found a wide range of applications and are commonly used as numerical displays in calculators and watches, as thermometers, in computer information displays,[3] in electronic games, and even as an artistic medium for paintings.[4]

There are three recognized classes of liquid crystals: smectic, namatic and cholesteric. Each class is distinguished by the way its individual molecules align. This article describes cholesteric liquid crystal compounds and how they might be used as large aperture optical isolators (or one way light valves) in the laser systems at LLE. Nematic compounds and their possible uses at LLE will be discussed in LLE Review #6.

All laser systems used to investigate inertial confinement fusion must focus their optical radiation onto small targets. Infrared

glass lasers like LLE's OMEGA risk damage to their optical components if infrared radiation reflected off a target surface is allowed to propagate back onto the laser system. Optical isolators are therefore placed at the output of each laser beamline. These devices permit light propagation only in a forward (to the target) going direction, acting as optical light valves to stop the propagation of any back reflected radiation. Three technologies capable of providing isolation are the Faraday rotator[5] (used on Shiva[6] at LLNL, Gekko IV[7] at Osaka, and on numerous other systems) the plasma shutter[8] (being developed for Nova at LLNL[9]), and the large aperture optical retarder (LAOR) currently used on OMEGA at LLE. The liquid crystal isolator[10] offers an attractive fourth alternative.

Unlike the Faraday rotator or plasma shutter, the liquid crystal isolator (LCI) is a passive device that requires no electronics, electric or magnetic fields, or synchronization with the firing of the laser system. It consists simply of a glass cell filled with a thin layer of liquid crystal material. Figure 4 shows schematically how the LCI works. Right-hand circularly (RHC) polarized infrared radiation generated from a laser system passes unattenuated through the LCI and propagates to the target. A portion of the light not absorbed by the target is specularly reflected and undergoes a 180° shift in its phase of vibration. The polarization sense of this retroreflected light is now left-hand circular (LHC), and the liquid crystal cell will not permit this state of polarization to pass.

Fig. 4
Schematic diagram of liquid crystal isolator. Liquid crystal cells may be used to provide protection of the laser system from back reflections from the target. In this illustration the liquid crystal cell is shown to pass right-hand circularly polarized (RHC) light to the target but will block the reflected left-hand circularly polarized (LHC) light.
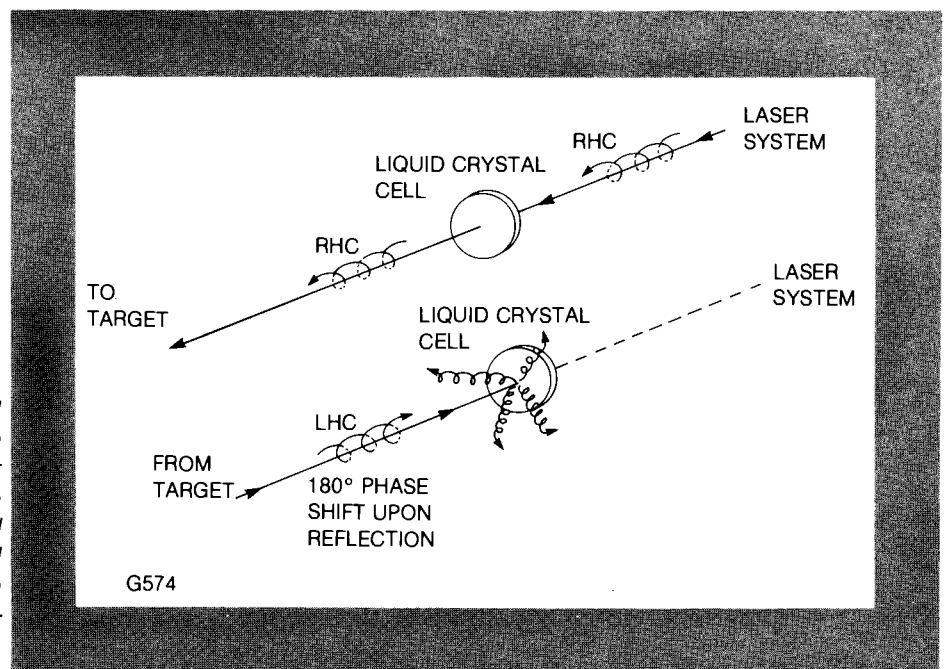
Advantages of the LCI include its large aperture capability; low optical loss for light propagating in the forward direction; high contrast ratio or blocking ability for backward propagating light; simplicity of fabrication, installation and operation; and low cost.

Fig. 5
Layered structure of cholesteric mole-cules. Cholesteric molecules are ar-ranged with their molecular dipole moments oriented from layer to layer in a helical screw sense. The helix pitch will vary depending on composition, temperature, and mechanical stress.
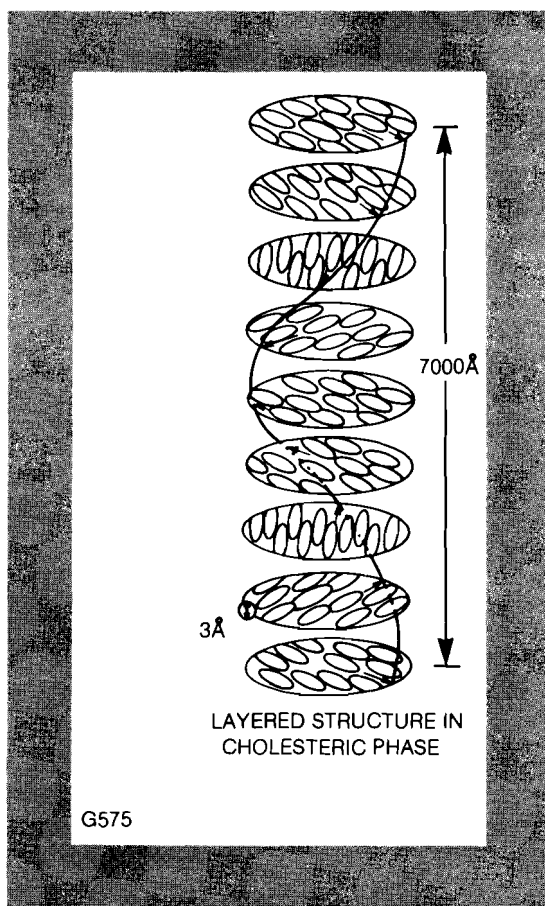
The circularly polarized output characteristic of LLE laser systems[11] is ideally suited for input to a LCI.

The principle of operation within the liquid crystal itself can be described by referring to Fig. 5. The cholesteric class of liquid crystals consists of long chains of carbon and hydrogen atoms, bonded together in a manner characteristic of the substance cholesterol[1] (hence their name). Additional side chains give each cholesteric molecule a rod-like shape roughly 0.3 nm in diameter and 3 nm long. Cholesteric liquid crystals form a layered structure when placed between flat glass plates. Within a given layer (see Fig. 5) all molecules preferentially align with the direction of their long axes (directors) parallel to each other. In the next layer, spaced some 0.5 nm away the molcules are likewise aligned with long axes parallel, but the protrusion of side groups forces the directors to be rotated some 10-30 minutes of arc away from that of the previous layer. Figure 5 shows that the directors (indicated every 150 layers within the cholesteric) trace out a helical path. The distance required for the directors to rotate 360° is called the pitch, p, of the cholesteric liquid crystal.

The helical screw-sense of the cholesteric liquid crystal phase is the key to the LCI's principle of operation. Light propagating up through the layers depicted in Fig. 5 with a sense of circular

Fig. 6
Wavelength of peak reflection for different 624/CN mixtures. The wavelength for peak reflection from a cholesteric liquid crystal combination can be varied by adjusting the ratio of the mixture.
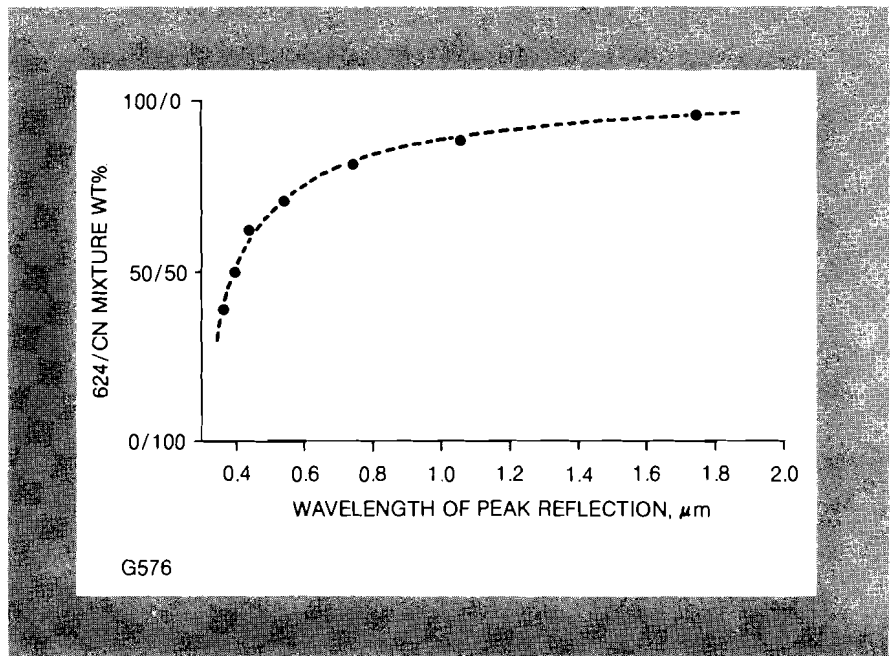
polarization opposite to that of the molecular helix will be transmitted unattenuated through the material. Light circularly polarized with the same screw-sense of the molecular helix will encounter constructive interference as it propagates from layer to layer,[4] eventually being totally reflected. This difference in transmittance for LHC versus RHC polarized light (called circular dichroism) is exhibited by the cholesteric only at a wavelength that satisifies the equation[12]

$$\lambda_{max} = n \text{ (index) } p \text{ (pitch)}$$

where n is the average refractive index of the liquid crystal. The wavelength of maximum selective reflection can be controlled easily by varying the pitch, p, through changes in liquid crystal composition.

Chemical stability with aging and temperature insensitivity are desirable for cholesteric compounds used in LCI cells. Figure 6 shows how, by varying the proportions of two commercially available left-handed cholesterics, one can tune the selective reflection peak into the infrared. A stable mixture tuned to $\lambda = 1.05\ \mu m$ has been used to fabricate a number of LCI cells for on-line tests at LLE.

A typical cell consists of a 12 μm thick layer of cholesteric liquid crystal material sealed between two externally AR coated 100 mm diameter optical glass windows. Measurements with the 64 mm rod output of the GDL laser system have found such cells to transmit 97% in RHC polarized light and 0.7% in LHC polarized light, thus providing a contrast ratio of better than 130:1. Separate tests have determined the 1.054 μm laser damage threshold of the cholesteric combination (see Fig. 6) to be greater than 20 GW/cm^2 at 700 psec. Cells have exhibited no degradation of optical properties over the past fourteen months.

In summary, the liquid crystal isolator offers an attractive alternative to presently used devices. LCI's are readily scalable to apertures larger than 100 mm, possess low insertion loss and good optical isolation, show minimal temperature sensitivity, and exhibit good long-term chemical stability. LCI's are passive devices, whose design simplicity could offer considerable cost advantages if implemented on a large aperture multiple beamline laser system.

REFERENCES
1. J. L. Fergason, *Sci Am* **311** (2), 77-85 (1964).

2. J. L. Fergason, *Opt. Spect.,* 54-59 (June 1978) and 42-46 (Sept. 1978).

3. F. J. Kahn and H. Birecki, *The Physics and Chemistry of Liquid Crystal Devices,* edited by G. J. Sprokel pp. 79-94 (1980).

4. D. M. Makow *Color Research and Application* **4** (1), 25-32 (1979).

5. See for example: C. F. Padula and C. G. Young, *IEEE J Quantum Electron* **QE-3,** 493-498 (1967); O. C. Barr, J. M. McMahon and J. B. Trenholme, *ibid.* **QE-9,** 1124-1125 (1973); and P. J. Brannon, R. R. Franklin, G. C. Hauser, J. W. Lavaske and E. D. Jones, *Appl. Opt.* **13,** 1555-1557 (1974).

6. *Laser Program Annual Report – 1976* (Lawrence Livermore Laboratory), pp. 2/85-2/87.

7. *Annual Progress Report on Laser Fusion Program – September 1977 – August 1978* (Institute of Laser Engineering, Osaka University).

8. I. F. Stowers, L. P. Bradley and C. B. McFann, *Topical Meeting on Inertial Confinement Fusion – Technical Digest* (OSA/IEEE), p. 128 (1980).

9. *Laser Program Annual Report – 1979* (Lawrence Livermore Laboratory), pp. 2/219-2/228.

10. S. D. Jacobs, J. A. Abate, K. A. Bauer, R. P. Bossert and J. M. Rinefierd, *Topical Meeting on Inertial Confinement Fusion – Technical Digest* (OSA/IEEE), p. 128 (1980).

11. W. Seka, J. Soures, O. Lewis, J. Bunkenburg, D. Brown, S. Jacobs, G. Mourou, and J. Zimmerman, *Appl. Opt.* **19,** 404-419 (1980).

12. J. L. Fergason, *Liquid Crystals,* edited by Brown, Dienes and Labes (Gordon and Breach), pp. 89-103 (1965).

Section 2
PROGRESS IN LASER FUSION

2.A Ultraviolet Experiments

In previous volumes of the LLE Review the rationale for using short wavelength lasers for fusion has been discussed. In volumes 2 and 3 some of the breakthroughs in frequency conversion technology made at LLE were presented. In this volume we discuss the initial 0.35 μm irradiation experiments performed in support of the national inertial fusion program.

Between September and November 1980 the GDL 0.35 μm irradiation facility became fully operational and initial experiments were performed. Modifications to the 1.054 μm system were completed in the summer and installation of the 0.35 μm conversion system was completed by the beginning of September. Extensive check-out work on the 0.35 μm laser diagnostics and frequency doubling and tripling conversion tests were performed during September. Subsequently, experimental work on 0.35 μm laser light absorption began followed by initial experiments using x-ray spectroscopy, stimulated Brillouin scattering, and plasma blow-off analysis with a Thomson parabola.

Figure 7 is a schematic layout of the ultraviolet irradiation system in its present state. The most essential elements are the conversion crystals, output energy and pulse (streak camera) diagnostics, and target focusing and viewing optics.

The expanded (130 mm diameter) infrared laser beam from GDL is frequency doubled and tripled in two 14 cm diameter type II
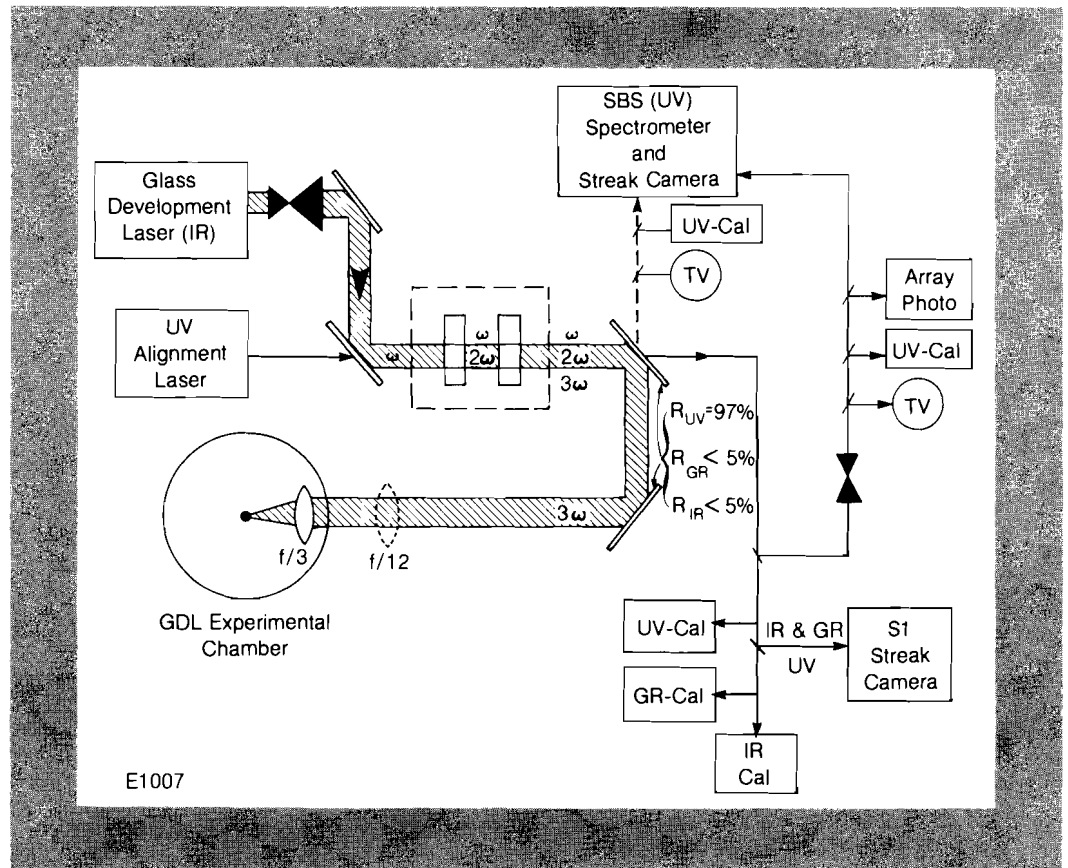
Fig. 7
Schematic GDL-UV layout. Beam paths
and diagnostics are shown for the infrared,
green, and ultraviolet laser beams in
GDL.

KDP crystals using a tripling scheme recently developed at LLE.[1] The two uncoated conversion crystals are 7.6 and 8.3 mm thick and reach maximum conversion efficiency at 1.054 μm input intensities of approximately 6 GW/cm², somewhat above the present laser output capabilities of 4 GW/cm² yielding overall energy conversion efficiencies of approximately 50 to 55% from the 1.054 μm to 0.35 μm output. Figure 8 illustrates predicted and measured conversion efficiencies for the present system.

UV as well as residual infrared and green output beam diagnostics are performed behind the first mirror after the crystals (see Fig. 7). This mirror reflects 97% of the UV via a second identical mirror towards the focusing optics and the target. The IR and green residual components and 3% of the UV are transmitted and their individual energies and temporal pulse shapes are measured using calorimeters and an S1 multiplexed picosecond streak camera. Typical streak camera traces are shown in Fig. 9. The UV pulse is narrower than either green or IR beams due to the lower IR-to-UV conversion efficiencies at lower power (intensity). The double-bumped IR pulse reflects the high conversion to UV at the peak of the pulse at which time the IR output pulse is significantly depleted. Intensity and time calibration for these traces are provided by calibration etalons (i.e. mirror pairs with 70% reflectivity).
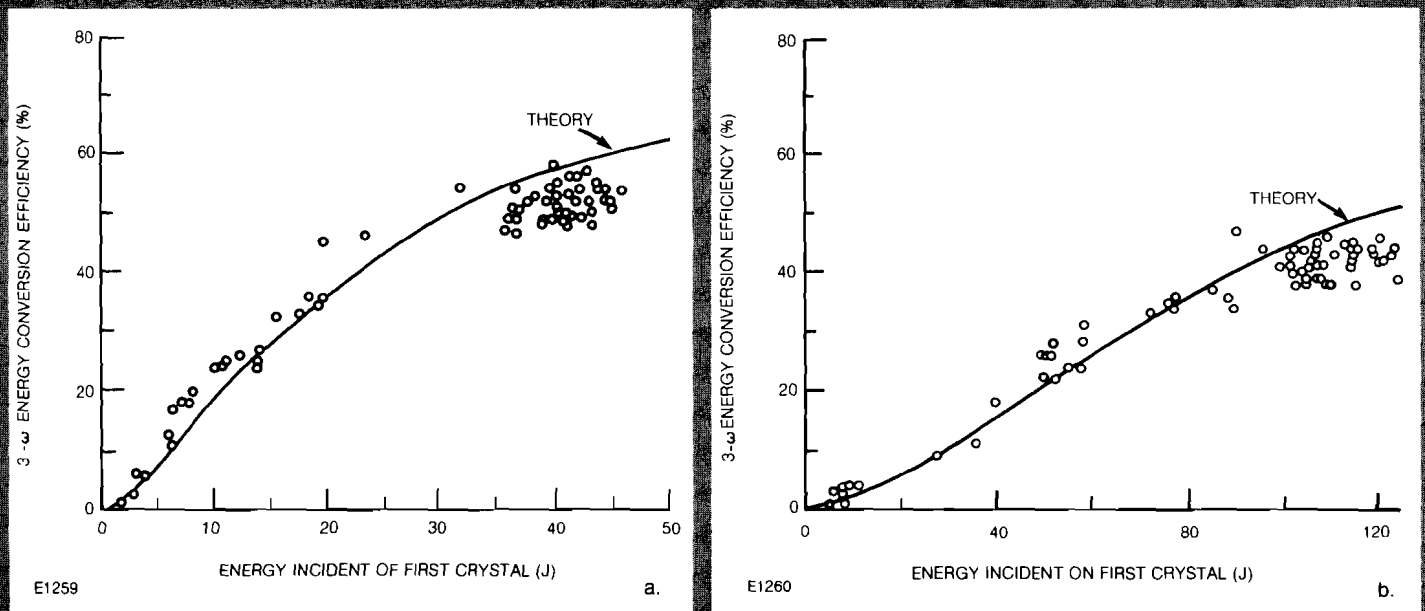
Fig. 8
Overall 3ω energy conversion efficiencies for (a) 135 psec and (b) 600 psec IR pulses. Theoretical curves include real beam cross sections, pulse shapes, and actual crystal length (7.6 mm KDP type II doubler, 8.3 mm KDP type II tripler).

The quality (intensity distribution and collimation) of the incident IR beam and output UV beam have been characterized using near field photography and shearing-plate interferometry. A typical IR beam cross section is shown in Fig. 10 indicating intensity fluctuations in the beam of less than 10%. The beam has been collimated to less that λ/2 in the UV. This also corresponds roughly to the uncorrectable divergence in the beam of approximately 50 μrad leading to a minimum focus, for the f/12 focusing lens, of 87 μm diameter. (In the future we will have at our disposal an f/2 lens with a minimum focus diameter of less than 30 μm).
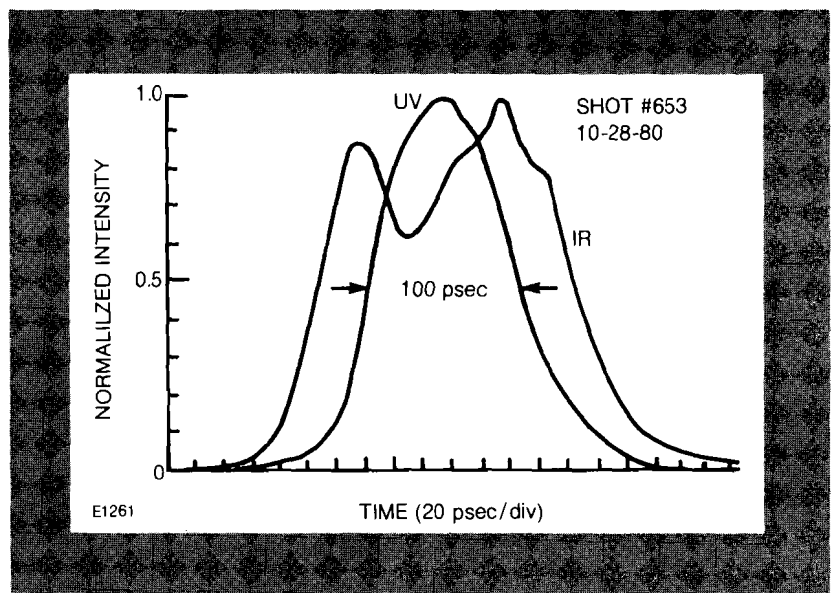

Fig. 9
Typical streaks of IR and UV output pulses from tripler. Minimum of IR pulse is due to high tripling conversion around the peak of the pulse.

The f/2 focusing lens allows us to irradiate targets with up to 5×10^{15} W/cm² while the f/2 lens will raise the maximum irradiation to the 10^{16} W/cm² range.

The performance of the UV irradiation facility is approximately 25 J at 100 psec and approximately 50 J at 400-500 psec - all measured in the UV. Infrared and green leakage on-target is typically below approximately 10^{-2} in energy while the IR and green on-target intensity is reduced to approximately 10^{-4} to 10^{-5} due to the chromatic shift in the focusing lens.

Fig. 10
Near field infrared beam cross section in front of doubling crystal. Near field photographs of the GDL infrared beam show good quality with beam intensity fluctuations of less than 10%.
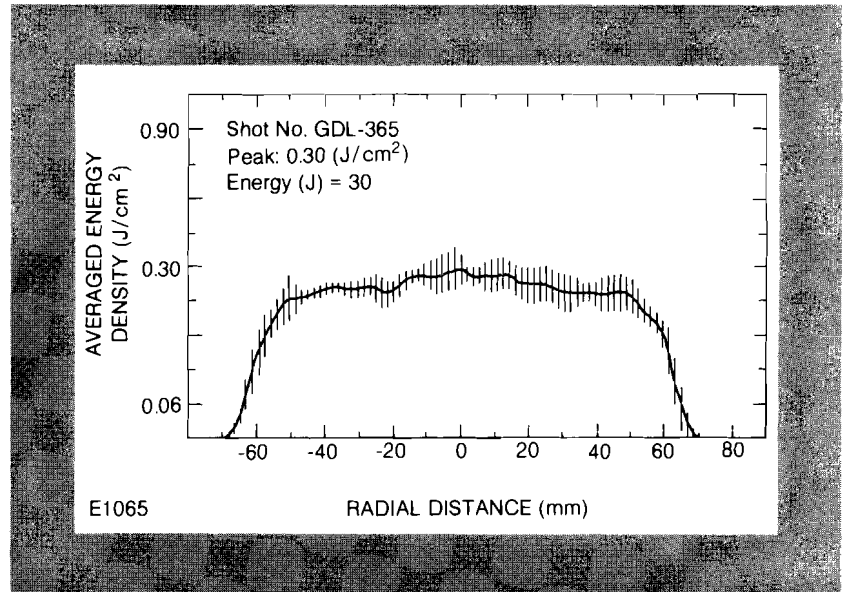
The UV experimental facility has been chosen to fulfill the needs of the UV interaction program which has as its main elements:
- Absorption: measurements and evaluation of relevant absorption mechanisms
- Electron transport: determination of inhibition of free streaming electron transport and
- Hot electron generation: determination of existence and importance of hot electron generation mechanisms.

Absorption measurements are made using a box calorimeter surrounding the target. The signals from this calorimeter can be analyzed in terms of contributions arising from the scattered light and from the blow-off plasma and x-rays. The former has a short-time response while the latter has a delayed response of several minutes after the shot. The plasma and x-ray signal is due to the purely radiative coupling between the ion shield and the sensors of the box calorimeter. By analyzing both signals a redundant measurement of the absorption can be made. Linear and non-linear laser light absorption in the ion shield is avoided through the use of a quartz (Suprasil™) ion shield whose transmission at 0.35 μm was periodically remeasured.

Between September and November 1980 the first absorption measurements were conducted. The box calorimeter yielded

results on absorption for short pulse (100 psec) irradiation between 10^{13} and 5×10^{15} W/cm². Some initial results have also been obtained for 400 psec pulses. We have observed absorption fractions between 60 and 95% (see Fig. 11) depending on pulse length and target material. Theoretical predictions made using 1-D (LILAC) and 2-D (SAGE) hydrocode have similar trends in the intensity dependence of the absorption and are also shown in Fig. 11.
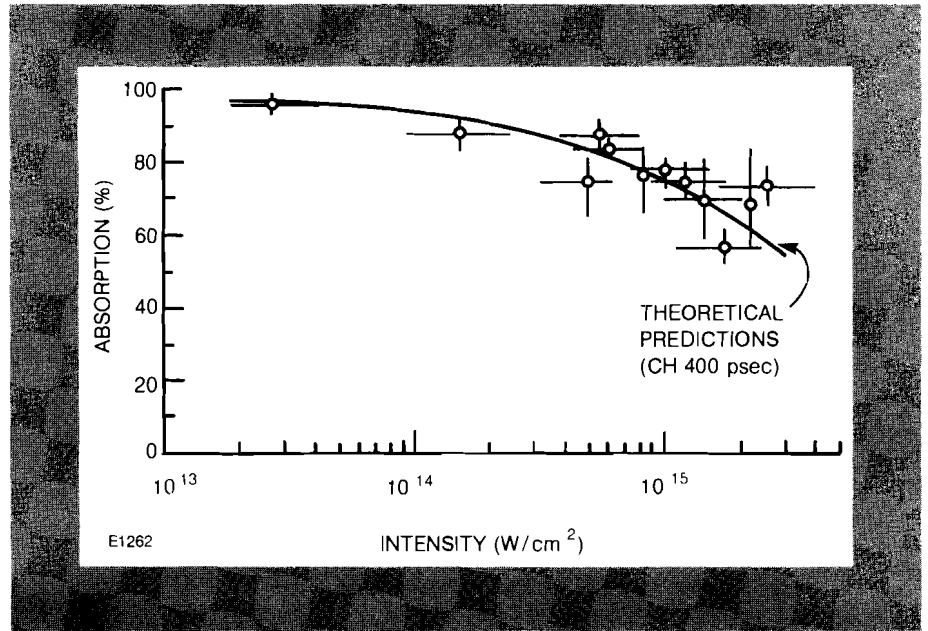

Fig. 11
Absorption of 450 psec 3ω light by plastic targets. Dashed line is calculated absorption assuming inverse bremsstrahlung and a flux limiter of f=0.03.

X-ray spectroscopy is being used to obtain information on heat transport in the following ways:

(a) For the plastic-coated glass targets we measure the reduction of silicon x-ray line intensity for increasing plastic thickness.

(b) For the teflon targets we measure the intensity and Stark broadening of F^{+8}, F^{+9} x-ray lines, both of which can be expected to increase for better heat transport into the super-dense plasma.

(c) Ti and Ni targets can yield information on transport in high-Z plasmas. Heat inhibition produces a higher temperature and therefore enhancement of high-Z ion lines.

Figure 12 shows some examples of the results. At 1.5×10^{14} W/cm² (400 psec pulses) a plastic layer thickness of about 4 μm resulted in a reduction of the silicon lines from the glass by an order of magnitude. As expected, Si^{+13} lines disappeared earlier than Si^{+12} lines. At 2×10^{15} W/cm² and 2×10^{13} W/cm², the corresponding thickness was 7 μm and 1-2 μm, respectively. For 100 psec pulses at 4×10^{15} W/cm² that thickness was 1-2 μm. Preliminary analysis with the 1-D laser fusion code LILAC indicates that a flux limiter f ~ 0.03-0.06 is required to model the results. A more accurate analysis is underway where the intensities of these x-ray lines are calculated using a rate-dependent model including radiation transport.

Fig. 12
Burn-through spectra of glass targets covered with different thicknesses of plastic. X-ray spectroscopy has been used to measure the burn-through depth of plastic coated targets irradiated with a 400 psec pulse of ultraviolet. The spectra are shown for (a) bare glass target, (b) 2 μm CH coated glass target, and (c) 4μm CH coated glass target. The 4μm CH coating reduced the intensity of the silicon line from the glass by an order of magnitude.
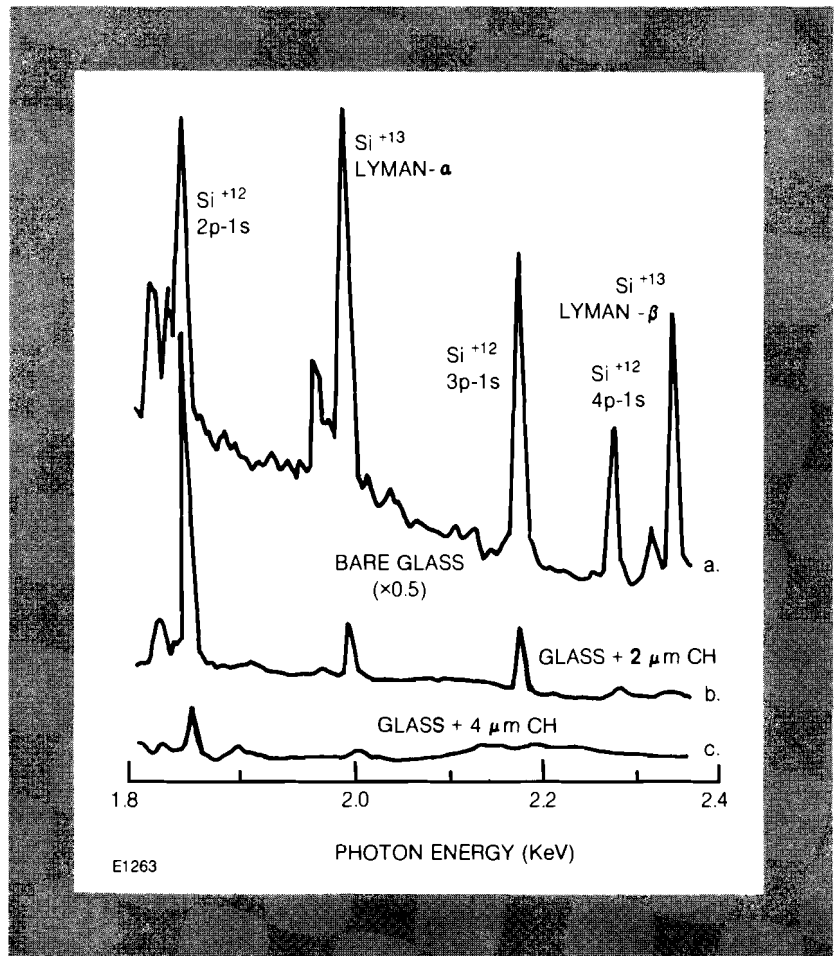
The results obtained from the teflon, Ti and Ni targets supplement the above measurements. The intensity of x-rays from the high-Z targets (0.12 J for the 4.7 KeV line of Ti^{+20}), the spectral width of fluorine lines and other spectroscopic signatures are incorporated into an analysis which will yield information on the thermal transport for targets of various materials.

In the coming months experiments using time-resolved x-ray emission and absorption will be used to obtain more detailed information on absorption and transport. In addition, measurements of the continuum x-ray spectrum will be conducted to determine the importance of suprathermal electron generation in short wavelength laser irradiation experiments.

REFERENCES

1. W. Seka et. al., *Opt. Comm.* **34** 469 (1980). R. Craxton, *Opt. Comm.* **34** 474 (1980).

2.B Nonlinear Evolution of Ablation Driven Rayleigh-Taylor Instability

Simulations of the Rayleigh-Taylor instability of ablatively accelerated thin-shell fusion targets show that the nonlinear evolution exhibits spike amplitude saturation due to ablative mass removal; the shell anterior surface evolves to a laminar (non-turbulent) quasi-stationary distorted state. The perturbed flow causes a significant departure from spherically symmetric behavior, but the laminar shell interior structure makes it appear possible to retain some of the advantages of larger aspect ratio fusion targets.

Spherically symmetric calculations of the behavior of laser-driven fusion targets have demonstrated major advantages of employing ablatively imploded spherical shells for obtaining optimum performance. The use of shells, as opposed to solid spheres, has been shown to reduce significantly the peak laser power required to drive successfully a target of fixed mass. In general it is predicted that performance improves with increasing shell aspect ratio, A $(\equiv r/\Delta r)$, where r and Δr are the initial radius and thickness of the shell,[1,2,3] and the useful range of A is approximately $5 < A < 100$. Unfortunately the continuous inward acceleration of a spherical shell by ablation pressure applied to its outside surface causes an instability which is a form of the Rayleigh-Taylor instability[4] and is capable of disrupting the spherical symmetry and subsequent thermonuclear burn enough to constitute failure. Extrapolations of linear stability theory predict failure in shells with A larger than some number near 5.[1,3,5] To make quantitative predictions of failure, we present nonlinear ablative calculations which show important departures from the classical nonlinear development of the instability.[6,7,8] In particular it is seen that (1) growth of the spikes tends to saturate, i.e. their growth rate decreases significantly at large amplitude and in some cases the spike structure becomes approximately stationary except for time-dependent ablative mass removal effects; (2) the spike structure resembles the classical case with an Atwood number, $\alpha = 1$,[7] in the sense that no Kelvin-Helmholtz structure is seen;[7,8] and (3) the flow is sufficiently distorted to cause significant departure from spherically symmetric behavior but exhibits a laminar (non-turbulent) structure. The results suggest the upper limit imposed by instability on the range of aspect ratios that can be used successfully may be extended to higher values than previously believed. Target reoptimization calculations will be required which consider the instability distortions and include the effects of converging geometry.

We study the nonlinear effects of the instability in a series of numerical simulations of a segment of a plane slab of fully ionized $Z = 6$ material accelerated between two rigid, parallel slip surfaces by ablation pressure. The ablation is driven by a constantly absorbed laser irradiance in the range $I = 2 \times 10^{14}$ to 10^{15} W/cm², deposited at a critical density of $n_e = 10^{21}$ cm⁻³.

These simulations could have been done in spherical geometry (finite A) instead of in planar geometry, ($A \rightarrow \infty$), but planar geometry avoids the choice of a particular A and makes identification of basic phenomena easier by eliminating convergence effects. The simulations were done with a two-dimensional triangular Lagrangian hydrodynamics code, DAISY, which includes nonlinear electron thermal conduction. The simulations employ 72 zones per perturbation wavelength. The resulting resolution is consistent with that required in recent Lagrangian simulations of the Rayleigh-Taylor instability of an incompressible inviscid fluid.[7]

The simulations were begun with an initially uniform shell density of 2 g/cm³ and thickness of 3μm, and run until a quasi-steady ablative flow is established near the shell surface. At this time t_i, the simulation is made two-dimensional, and the instability is initialized by imposing a divergence-free perturbation of the form

$$\overline{\xi} = \overline{\nabla} \times (\hat{z}A_z),$$

$$A_z = (\xi_o/k_y) \sin (k_y y) \operatorname{sech} k_y(x\text{-}x_m).$$

Here x is the direction of slab motion, y runs parallel to the slab, and x_m is the point of maximum shell density. The unperturbed calculations show that the slab would be consumed by ablative mass removal at a burn-through time of about $t_B = 140$ psec.

To determine which unstable cases are most interesting, linear instability growth rates γ (k_y) were obtained from the planar stationary flow model of ablation[10,11] and compared with the 2-D simulation results. In the 2-D calculation, the initialization procedure described above was used with $\xi_o/\lambda_y = 0.01$. Figure 13 shows a
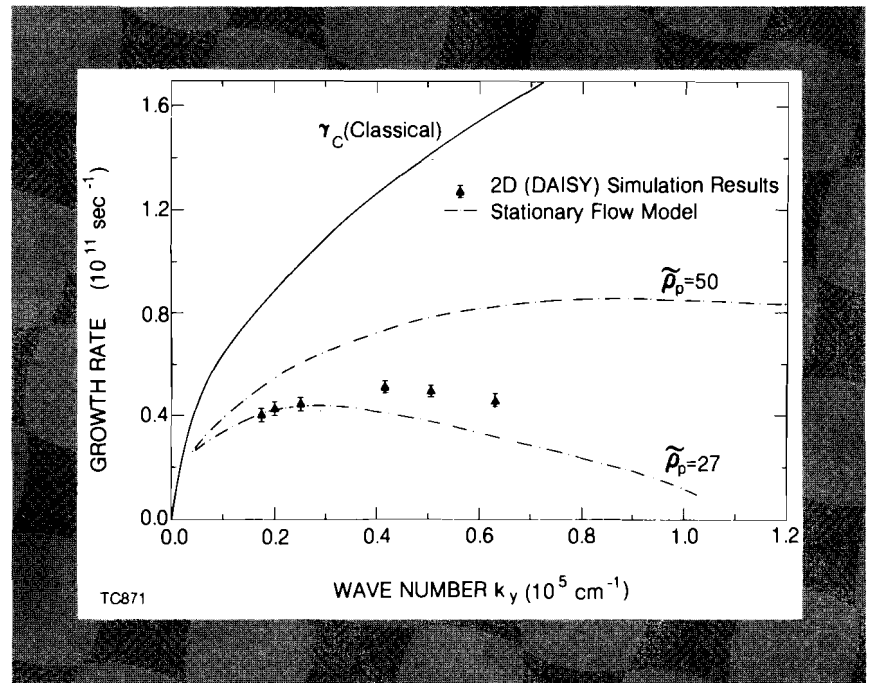

Fig. 13
Comparison of the 2D simulations of Rayleigh-Taylor linear instability growth rates with the stationary flow model.
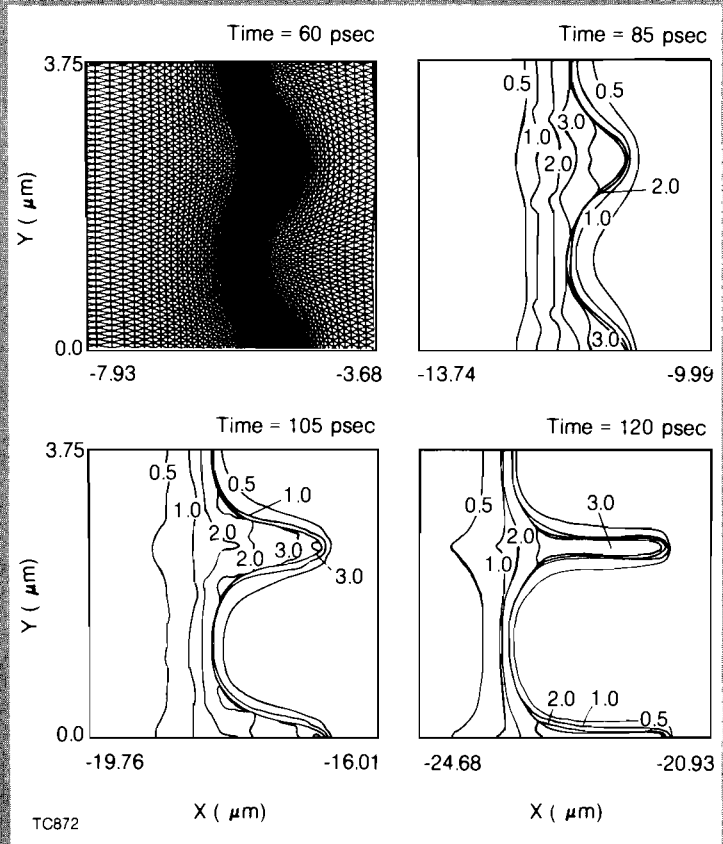
Fig. 14
Initial mesh configuration at 60 psec
$(k_y \xi_o = \pi/5)$ *and time evolution of the*
density contours for the $I = 10^{15}$ *W/cm²,*
$\lambda_y = 2.5$ μm *case.*

set of values of $\gamma(k_y)$ obtained with the 2-D code from an

$$I = 10^{15} \text{ W/cm}^2$$

zeroth order solution initialized at t_I, and $\gamma(k_y)$ obtained from the stationary model.[11] The stationary solutions are characterized by a single parameter, the ratio of maximum density to the isothermal sonic point density $\tilde{\rho}_p$. The simulated results are not quite stationary but correspond closely to values of $\tilde{\rho}_p \sim 27$ and are bounded by $27 \leq \tilde{\rho}_p \leq 50$ (see Fig. 13). For comparison the classical growth rates, $\gamma_c \equiv (k_y \ g)^{1/2}$ are shown. Ablative effects cause $\gamma(k_y)$ to reach a maximum and then decrease to zero with increasing k_y, in contrast with γ_c which increases indefinitely (Fig. 13).[1,12] This result is consistent with previous time dependent perturbation solutions.[1,13] The potentially troublesome and interesting range of k_y is near the maximum of $\gamma(k_y)$ and near the inverse of the shell thickness. The case $I = 10^{15}$ W/cm² and

$$k_y = 2.5 \times 10^4 \text{ cm}^{-1} \ (\lambda_y = 2.5 \ \mu m)$$

is seen from Fig.13 to be near the maximum, and was chosen, together with the

$$k_y = 6.2 \times 10^4 \text{ cm}^{-1} \ (\lambda_y = 1.0 \ \mu m)$$

case, to study the nonlinear development of the instability.

Figure 14 shows a time sequence of density contours from a run which began with the initialization shown in the first frame $(k_y \xi_o = \pi/5)$. This amplitude-to-wavelength ratio is one for which linear stability analysis is valid[7,8] initially. As the amplitude increases, structure is seen which resembles the classical Rayleigh-Taylor "bubble and spike"[6,7,8] phenomena but unlike the classical behavior the spike does not grow indefinitely due to ablative mass removal. This is also seen in the sequence of
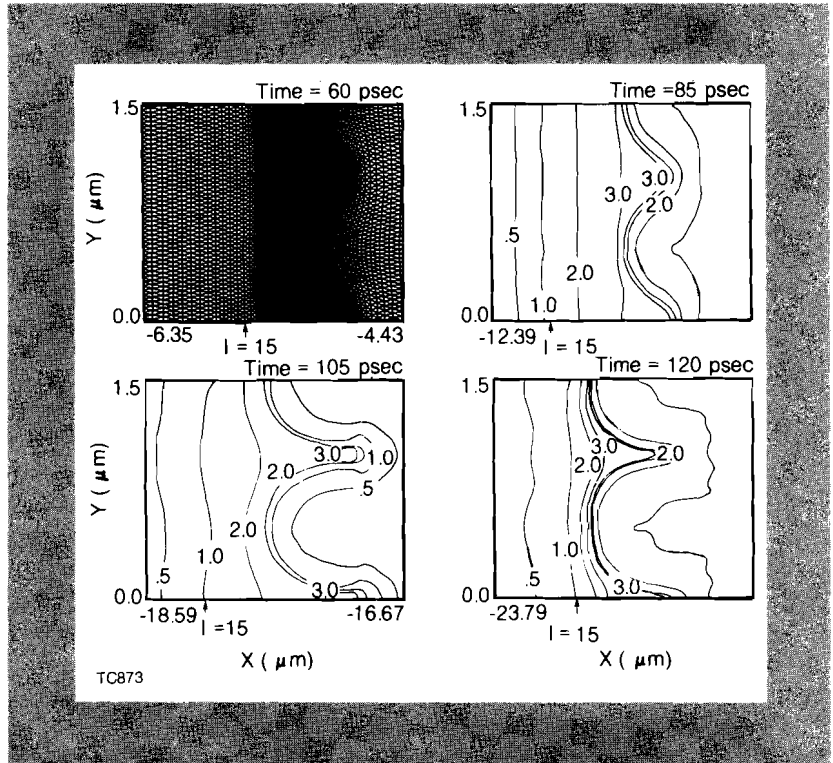

Fig. 15
Initial mesh configuration at 60 psec $(k_y \xi_o = \pi/5)$ and time evolution of the density contours for the $I = 10^{15}$ W/cm^2, $\lambda_y = 1.0$ μm case.

contours (Fig. 15), from the 1 μm run. In Fig. 16 a superposition of $\rho = 2$ g/cm^3 contours for the Fig. 15 case is shown. The $\rho = 2$ g/cm^3 contour was chosen to represent the approximate position of the shell surface (ablation front) because the density gradients are largest in the neighborhood of this density. Figure 17 gives the amplitude time history of the surface distortion (defined as the separation between the bubble and the spike for the $\rho = 2$ contours). In Fig. 17 a period of exponential growth (from about 70 to 95 psec) is followed by decreased growth at an amplitude slightly less than the wavelength, followed (for the 1 μm case) by a decrease to a smaller amplitude until burn through (about 140 psec). From Fig. 16 it is seen that as the spike approaches its maximum amplitude it becomes more narrow near the tip and then broadens again as its amplitude decreases while the bottom of the bubble is seen to become progressively flatter. Figure 17 also illustrates the relative thickness of the shell at its thinnest region (top of the bubble) for the two unstable cases, together with the unperturbed ablated shell thickness. The 2.5 μm case is the most globally disruptive. From Figs. 14 and 15 it is

interesting that a quasi-stationary distorted state does not evolve into a further state of turbulent mixing.[9] The cause of the saturated amplitude of the spike is seen to be the higher ablation pressure near the tip caused by the higher temperature there than at the same density in the bubble. Contour plots of temperature (not included) show this difference. The temperatures near the tip are larger because the tips are nearer to the heat source (the critical surface is located outside and to the right of the countour plots). Interestingly,the simulations show that the center of mass motion of the shell is virtually unchanged by the presence of the unstable Rayleigh-Taylor flow. The disruptive nature of the instability is apparent from Fig. 17. The instability evolves due to a nearly constant bubble rise velocity which removes mass from the bubble region. Particle paths from the simulations (not illustrated) indicate that the shell thickness near the bubble decreases linearly with time. The laminar nature of the flow is illustrated by the time-independent ordering of the density contours (Figs. 14 and 15).
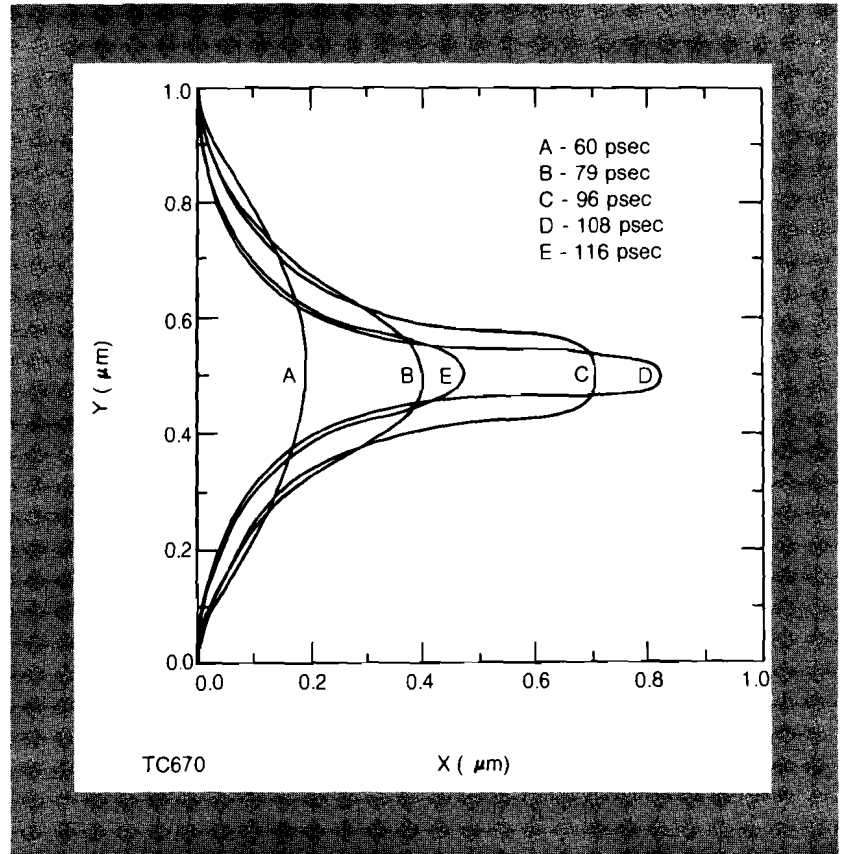

Fig. 16
Spike (p = 2 g/cm³ contours) at various times for the instability illustrated in Fig. 15.

We summarize by noting the form that the modes have acquired (last frames of Figs. 14 and 15) are sufficiently distorted to be a potential source of disruption of the final fuel compression of a large aspect ratio spherical fusion target. However, in both cases the left side of the shell, which is the side away from the laser and would correspond to the "inside" of a spherical shell, is seen to

Fig. 17
Spike amplitude as a function of time for the unstable cases of Figs. 14 and 15, and shell thickness at the bubble center as a function of time for the two perturbed cases compared with the unperturbed simulation.
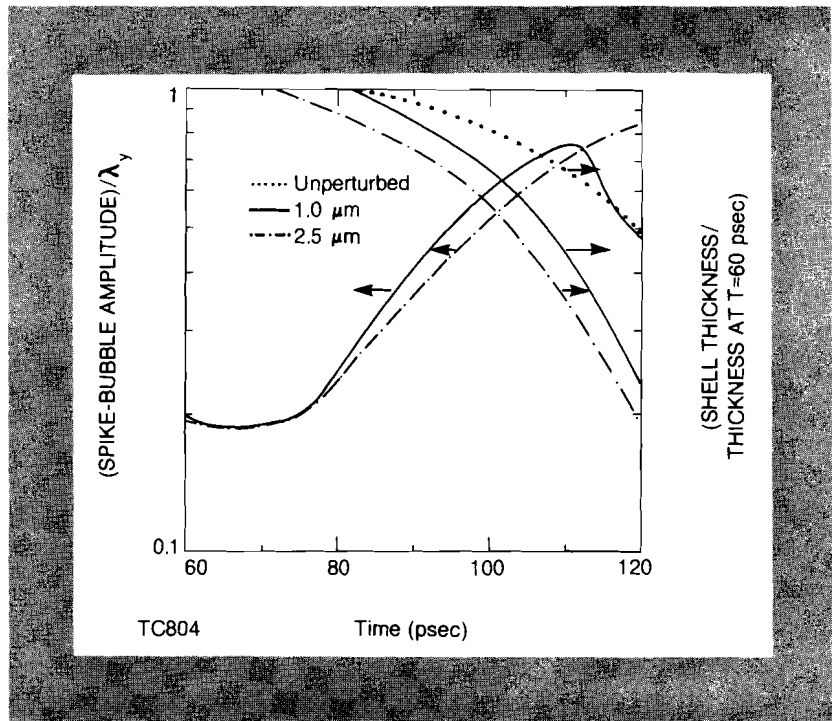
be less distorted than the outside. This laminar and only moderately distorted inner surface, while not as desirable as a perfectly flat (or spherical) surface, would in general not be mixed with lower density fuel inside it. In Fig 15 we illustrate this effect by marking a Lagrangian surface ($l = 15$) whose position at t_i corresponds to a material density near 0.8 g/cm^3 (about the density of shocked liquid D-T fuel). Consequently, somewhat better final fuel compression would be expected than if the inner surface of the shell had lost its integrity due to turbulent mixing. It therefore appears plausible that successful large aspect ratio ICF implosion systems may be designed to operate with shell distortions of the kind and amplitude seen here.

REFERENCES

1. G. Fraley, W. Gula, D. Henderson, R. McCrory, R. Malone, R. Mason and R. Morse, Plasma Phys. and Controlled Nuc. Fusion Research, **543**, (International Atomic Energy Agency, Vienna, Austria, 1974).

2. R.J. Mason, Nuc. Fusion, **15**, 1031 (1975).

3. Yu Afanas'ev et. al., Pis'ma Zh. Eksp. Teor. Fiz. 21, 150 (1975) [JETP Lett. 21, 68 (1975)], and Pis'ma Zh. Eksp. Teor. Fiz. 23, 617 (1976) [JETP Lett., 23,566 (1976)].

4. S. Chandrasekhar, Hydrodynamic and Hydromagnetic Stability, (Oxford U.P., Oxford, 1961), Chap. X.

5. R. L. McCrory and R. L. Morse, Phys. Fluids, **19**, 175 (1976).

6. J. D. Lindl and W. C. Mead, Phys. Rev. Lett. **34**, 1273 (1975).

7. G.R. Baker, D. I. Meiron and S. A. Orszag, Phys. Fluids **23**, 1485 (1980).

8. (a) F. H. Harlow, J. E. Welch, *Phys. Fluids* **9**, 842 (1966), (b) B. J. Daly, *Phys. Fluids* **10**, 297 (1967), (c) J. R. Freeman, M. J. Clauser and S. L. Thompson, *Nuc. Fusion* **17**, 223 (1977).

9. G. Birkhoff, Los Alamos Scientific Laboratory Report LA-1927 (1956) and LA-1862 (1955), unpublished.

10. S. J. Gitomer, R. L. Morse, and B. S. Newberger, *Phys. Fluids* **12**, 234 (1977).

11. (a) L. Montierth, F. L. Cochran, and R. L. Morse, *Bulletin of the American Physical Society* **24**, 945 (1979) and (b) R. L. McCrory, L. Montierth, R. L. Morse and C. P. Verdon, "Taylor Instability in Fusion Targets" in *Laser Interactions and Related Plasma Phenomena*, Vol. V, (Plenum Press, in press, 1980).

12. S. E. Bodner, *Phys. Rev. Lett.* **33**, 761 (1974).

13. R. L. McCrory, R. L. Morse, and K. A. Taggart, *Nuc. Sci. Eng.* **64**, 163 (1977).

2.C Enhanced Reflectivity Due to Pondermotive Rippling

Recent theoretical studies have elucidated a physical process which may play a significant role in determining the amount of light reflected from a target plasma corona. Unlike well-known scattering instabilities such as Stimulated Brillouin Scattering (SBS) and Stimulated Raman Scattering (SRS), this effect is due to an equilibrium feature of the coronal plasma flow.

The effect may be described using the simple model of the target plasma shown in Fig. 18. For simplicity, the light is taken to be normally incident (the extension to oblique incidence is straightforward). The corona is modeled by a uniform plasma of density n moving through the critical surface at a constant velocity v. To model the absorption processes, which are most effective near critical density, we assign the critical surface a partial reflectivity $R_0 < 1$. The incident light has wavenumber k; in combination with the light reflected from the critical surface it forms a standing wave of wavenumber $2k$. The electric field of this standing wave then gives rise through the pondermotive force to a stationary density ripple in the corona, also of wavenumber $2k$, which can Bragg-reflect the incident light and thus enhance the reflectance of the corona. A linearized analysis gives the following equation for the total reflectance R_{tot} due to the critical surface and the density ripples:

$$R^2_{tot} = R^2_o \, e^{\beta(1-R^2_{tot})}.$$

The parameter β contains the laser and plasma parameters

$$\beta = \frac{1}{4} \; \frac{n/n_c}{1-n/n_c} \; \frac{v/c_s}{[(v/c_s)^2 -1]^2 + \left(\frac{vv}{2kc^2_s}\right)} \; \frac{V^2_{osc}}{V^2_{th}} \; \frac{vL}{c_s}$$
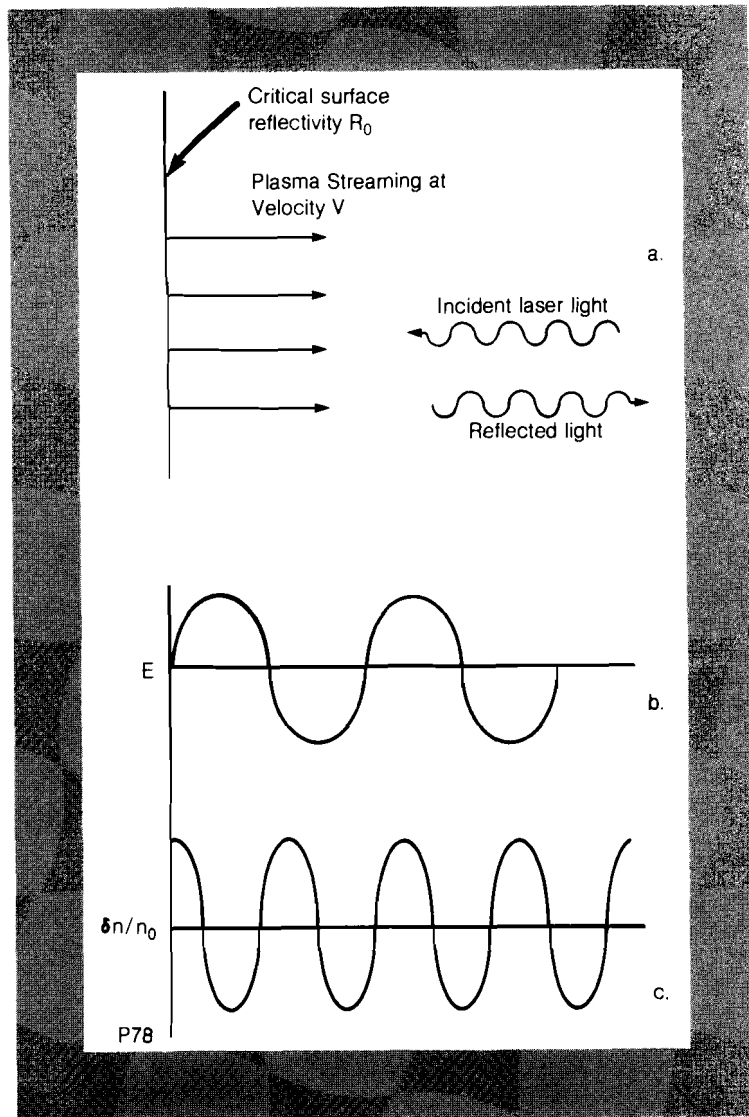
Fig. 18
Simplified model of corona. The incident laser light is taken to be normally incident to the uniform underdense plasma (a). The plasma is streaming at velocity v with respect to critical surface. Also shown are (b) the standing wave part of the electric field, wavelength K; and (c) the density fluctuations due to pondermotive force, wavelength 2k. These density fluctuations can Bragg-reflect the incident light.

Here n_c is the critical density, c_s is the ion sound speed, V_{osc} is the electron quiver velocity in the incident light, V_{th} is the electron thermal velocity, L is the length of the plasma, and v is a phenomenological damping factor, representing primarily ion


	INCIDENT LASER POWER (W/cm^2)		
	10^{14}	10^{15}	10^{16}
$T_e/T_i = 10$	$\beta = 0.938$	9.38	93.8
15	0.251	2.51	25.1
20	0.101	1.01	10.1

Values of β for L $=100$ μ, $v/c_s = 1.5$,
$n/n_c = 1.5$, $\lambda = 1.05\,\mu$

P81

Table 2
Typical values of β in a laser plasma corona.

Fig. 19
Total reflectance as a function of β and R_o ($R_{tot} \rightarrow R_o$ as $\beta \rightarrow o$). Density fluctuation may significantly enhance reflection from the corona for much of the parameter region of interest to laser fusion, $\beta > 1$.
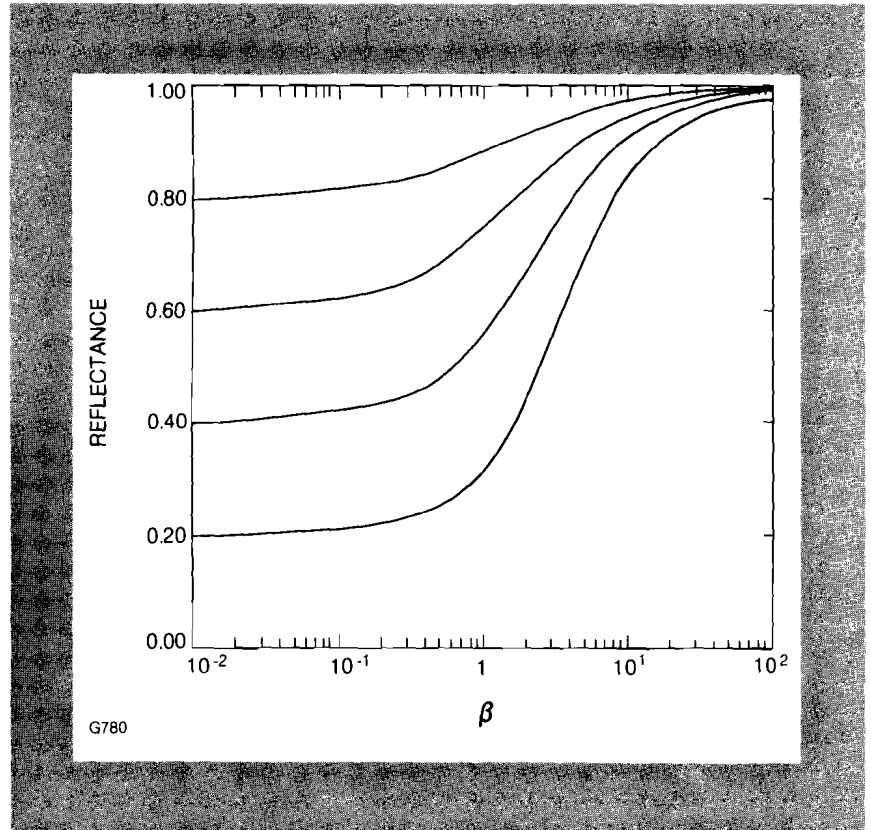
Landau damping. Note that if $v = 0$ or $v = 0$, $\beta = 0$ and $R^2_{tot} = R^2_o$. Thus both damping and a non-zero flow velocity must be present to obtain enhanced reflection from the coronal density ripples.

Results for R_{tot} as a function of β are shown in Fig. 19 for several values of R_o, the critical surface reflectivity. Note that for $\beta \ll 1$, $R_{tot} \sim R_o$, while for $\beta \gg 1$, $R_{tot} \simeq R_o \simeq 1$. The transition between these two limits occurs near $\beta = 1$, so that for $\beta < 1$ we expect significant enhanced reflection. In Table 2 are listed some typical values for β in a laser plasma corona, calculated for

$$L = 100 \ \mu m, \ v/c_s = 1.5, \ n/n_c = 0.5, \ \lambda = 1.05 \ \mu m,$$

and several values of T_e/T_i (ratio of electron to ion temperature) and incident laser power. The strong dependence on T_e/T_i is due to the Landau damping factor v in β. Table 2 shows that for much of the parameter region of interest to laser fusion $\beta > 1$, so that the density ripples may significantly enhance reflection from the corona.

Enhanced reflection is difficult to observe experimentally, since unlike SBS and SRS it does not alter the spectrum of the reflected light but rather augments the specularly reflected component. However, the density ripples themselves appear in simulations[1] and have been observed in microwave experiments[2]. When the coronal flow velocity is near the ion sound speed, the density ripples become ion acoustic waves and contribute to SBS[3].

REFERENCES

1. K. Lee, D. W. Forslund, J. M. Kindel, and E.L. Lindman, *Phys. Fluids* **20**, 51 (1977).

2. H. E. Huey, A. Mase, N.C. Luhmann, W. F. DiVergilio, and J. J. Thomson, *Phys. Rev. Lett.* **45**, 795 (1980).

3. C. J. Randall, J. J. Thomson, and K. G. Estabrook, *Phys. Rev. Lett.* **43**, 924 (1979), C. J. Randall, J. A. Albritton, and J. J. Thomson, UCRL-84330.

Section 3
DEVELOPMENTS IN
MICROFABRICATION

3.A Consolidation of Target Group at LLE

During this period the last phase of the transfer of the target development laboratory from the Exxon Research Laboratories at Linden, New Jersey, to LLE was completed. All activities associated with fusion target and materials development are now performed in the consolidated target fabrication laboratories at LLE.

Concurrent with the consolidation of target fabrication activities at LLE, a re-organization of this program has taken place. The new group leader for target fabrication is Dr. John Miller formerly of Los Alamos National Scientific Laboratory. Recent additions to the group include Dr. Merle Hirsh from the University of Minnesota and Dr. Hyo-Gun Kim from the Allied Chemical Corporation. The group now has eleven full-time and two part-time members.

Some of the current capabilities of the target fabrication laboratories include:
- Physical vapor deposition facility
- Photolithography facility
- Reactive ion etcher
- Polymer coater (parylene process vapor phase coater)
- Scanning electron microscopes – an Amray 1000A capable of 100,000X magnification with resolution of 15 nm and an ISI Super II with magnification of 65,000X
- Extensive optical microscopy capabilities including a

number of stereo microscopes, compound microscopes and interferometric microscopes
- Micro balances
- Laser hole drilling apparatus
- Micro assembly work stations

The addition of a new target fabrication facility designed specifically to accomodate the specialized activities associated with inertial fusion target production is currently in the preliminary design phase.

3.B Zone Plate Fabrication

The production of significant fluxes of suprathermal electrons is evidenced in laser fusion experiments by the generation of suprathermal x-ray radiation. This results from bremsstrahlung produced by radiative interactions between these electrons and thermal ions. Since this emission is Z dependent, it can be utilized to identify regions of the target in which significant suprathermal electron deposition occurs. Zone plate coded imaging[1] offers distinct advantages over alternate imaging techniques such as pinhole photography and grazing incidence microscopy, both from the point of view of spectral resolution and light gathering power. However, spatial imaging of the target in the hard x-ray region, typical of short pulse, high intensity exploding-pusher type experiments, requires coded aperture zone plates of thickness sufficient to resolve x-ray emission in excess of 10 KeV[2]. The intent of the present work was the production of zone plates thick enough to image x-rays in the 30 KeV range. This requires zone plates of Au with thicknesses in excess of 25 μm.

Zone plate fabrication begins by making a free standing negative mold, which is filled with gold by electroplating. Previous efforts[3,4] have used standard photolithographic pattern delineation methods. However, this approach encounters considerable problems in its application to the fabrication of thick zone plates having high aspect ratios. Ciarlo and Ceglio[4] have succeeded in delineating patterns in photoresist as thick as 40 μm, but many problems occur in this thickness regime. For example, cracks and bubbles can occur during UV exposure, and resist layers can exhibit thickness nonuniformities. In principle, these problems can be overcome with proper care in processing. A more fundamental problem is zone tapering, which is due to diffractive spreading of the exposure illumination by the fine details in the photomask. The maximum aspect ratio (thickness:linewidth ratio) achieved by the standard technique is about four, while zone plates with aspect ratios as high as ten would prove useful for imaging experiments.

Because of the problems inherent in thick photoresist processing, we have taken a different approach to ultrathick pattern delineation,

27

Fig. 20
Schematic representation of the reactive
sputter etching apparatus. Positive ions
are accelerated toward the cathode,
where they react chemically with the
sample to form volatile products.
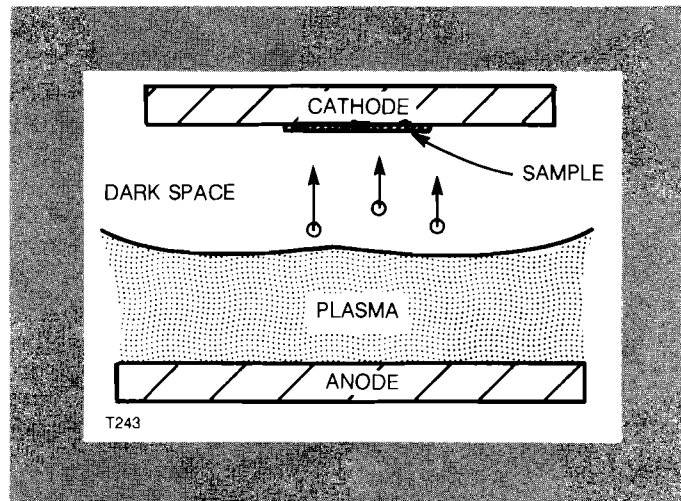
which uses reactive sputter etching (RSE).[5] Figure 20 is a
schematic of the RSE apparatus. A radio frequency discharge is
employed to sustain a plasma in a gas which is being pumped
through a chamber at low pressure. The specimen to be etched is
placed on the cathodic electrode. The gas is chosen such that it
will chemically react with the specimen, creating volatile reaction
products which are pumped away by the vacuum system.
Organic media can be reactively etched by oxygen at rates
approachng 250 nm/min.[6] RSE is just one of a family of so-called
dry etching methods. The exact mechanisms in the RSE process
are not completely understood, but RSE is known to be somewhat
material specific (due to its chemical nature) and highly directional
(presumably due to the acceleration of "reactive ions" in the
discharge) as well. These properties make it possible to vertically
etch high aspect ratio structures into polymers.

Crucial to this method of pattern delineation is the choice of the
polymer and mask material such that the RSE step will etch only
the polymer. This polymer must also be capable of being
deposited in thick uniform layers and able to withstand the
processing steps which follow pattern delineation, including
gold plating and wet-chemical etching (to remove metals). In
addition, since an integral mask is required, it must be possible to
deposit a metal film which does not etch, such as aluminum, with
excellent adhesion to the polymer.

Initially an attempt was made to find a polymer which could be
deposited on a gold substrate, but to date all of the materials we
have tried have failed to meet at least one of the requirements
discussed above. Consequently, we have adopted the somewhat
different procedure outlined in Fig. 21. Since we were interested
in zone plates approximately 50 μm thick, we began with a piece
of standard 2 mil Mylar™. Both sides of the Mylar™ were then
coated with approximately 0.2 μm of Al. One surface was then
coated with approximately 0.2 μm of Au. The gold surface was
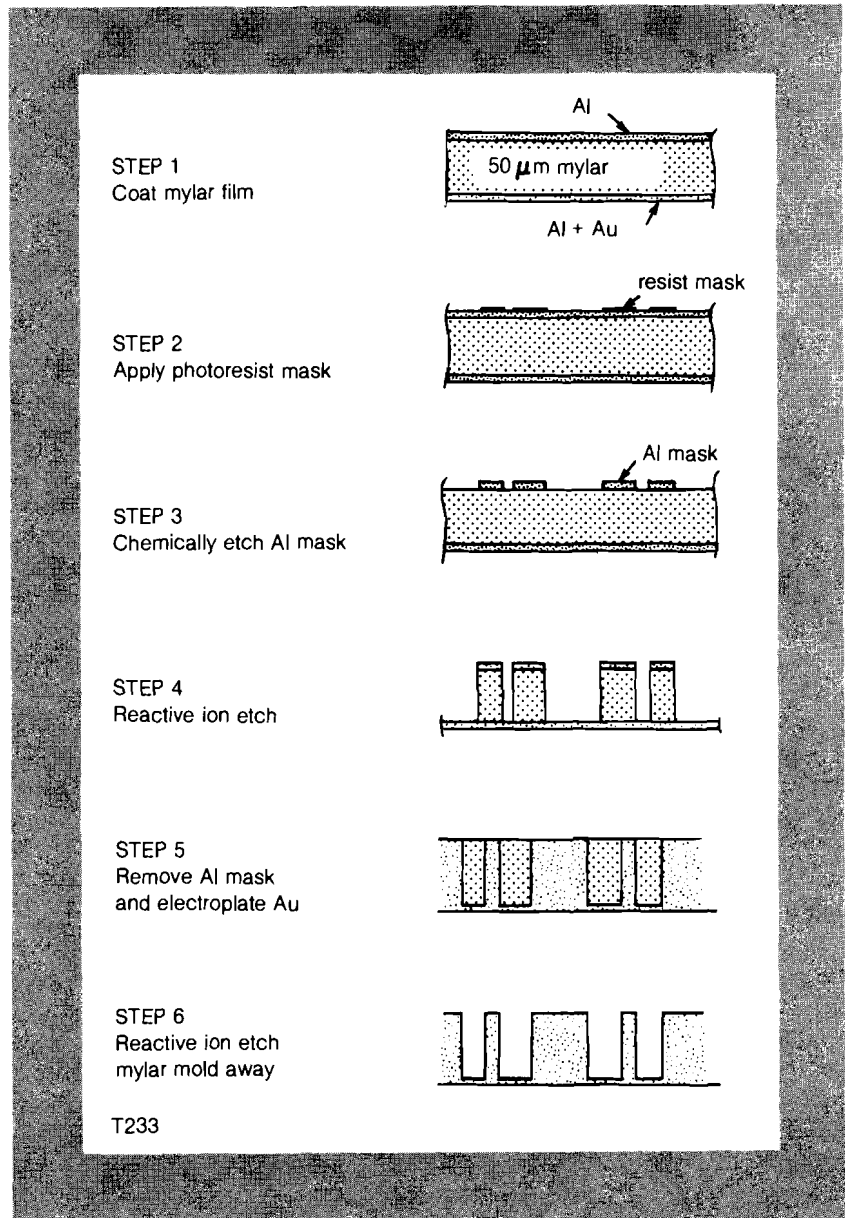epoxied to a glass cover slip, which offered the support necessary

Fig. 21
Zone plate fabrication. This sequence uses reactive sputter etching to form the mold.

for the subsequent steps. A thin layer of photoresist was spun on the aluminum surface, and exposed to UV light through the zone plate mask. After developing the resist, the exposed aluminum was chemically etched away, leaving an integral aluminum mask on the Mylar™. The masked Mylar™ was then put in the RSE and etched in oxygen, at a power of 0.28 W/cm², down to the Al (aluminum) layer on the back surface. This layer, which served to protect the gold during reactive sputter etching, was then chemically etched away. Gold was then electroplated into the mask, and the gold-Mylar™ combination was mounted on a ring. The final step consisted of placing the zone plate in the RSE and etching away the Mylar™.
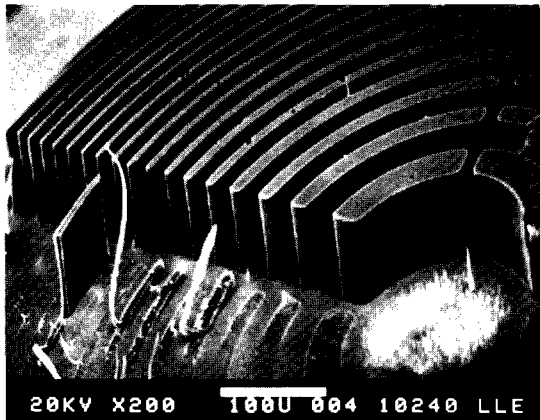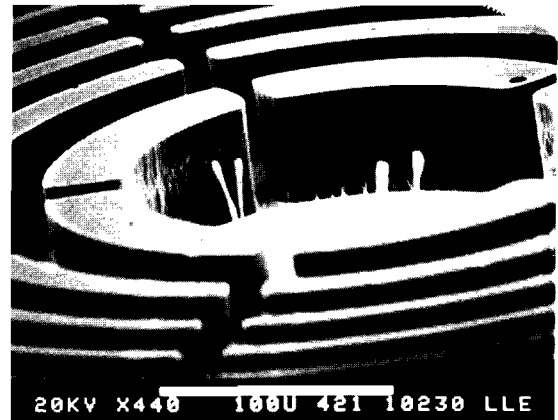
Fig. 22
Scanning electron micrographs of a mylar zone plate mold made by using reactive sputter etching. Significant improvements in aspect ratio have been obtained with this technique.

Figures 22(a) and 22(b) show scanning electron micrographs of a zone plate made by this method, and Fig. 23(a) and 23(b) show a finished gold micro-Fresnel zone plate. The thickness of this zone plate is 40 μm, and the outer zone width is 15 μm. Further work will probably make it possible to find mold materials that have the needed properties and which can be applied in layers of varying thicknesses. In addition, fabrication of zone plates of similar thickness to that shown in Fig. 21, but with a greater number of zones is now in progress.

REFERENCES

1. N. M. Ceglio et al., J. Appl. Phys. **48**, 1563 (1977); **48**, 1566 (1977), Phys. Rev. Lett. **39**, 20 (1977).

2. N. M. Ceglio and J. T. Larsen, Phys. Rev. Lett. **44**, 579 (1980).

3. Ceglio and Smith, Rev. Sci. Instrum. **49**, 15 (1978).

4. Ciarlo and Ceglio, Proceedings of SPIE Symposium on Semiconductor Microlithography, San Diego, March 1980.

5. Lehmann and Widmer, J. Vac. Sci. Technol. **15**, 319 (1978).

6. Goldstein and Kalk, J. Vac. Sci. Technol., Jan./Feb., 1981 (to be published).

Fig. 23
Scanning electron micrographs of a completed gold micro-Fresnel zone plate. The thickness is 40 μm, and the outer zone width is 15μm.
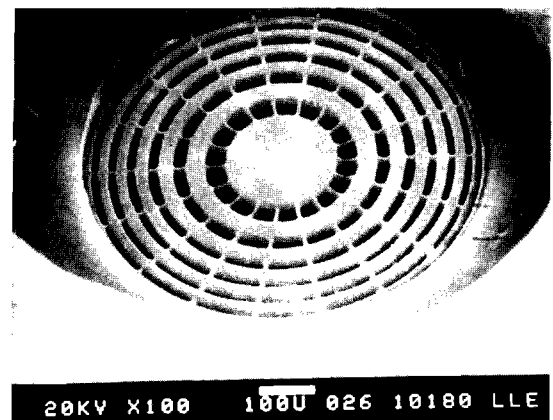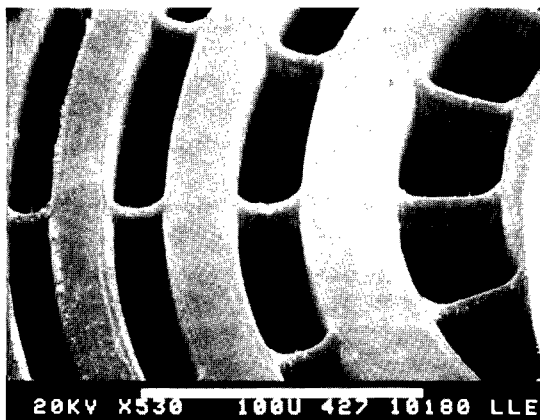
Section 4
DEVELOPMENTS IN
SUBPICOSECOND RESEARCH

4.A A New Picosecond Pulse Source

Subpicosecond pulse generation is currently achieved with either passive mode-locking or synchronous pumping.[1,2,3,4,5] Synchronous pumping with an argon laser pump is generally preferred because of its simplicity. Amplification of the picosecond pulse is adversely affected, however, by the lack of an accurate synchronization of the oscillator and the amplifier.

We have obtained picosecond pulses from a synchronously pumped CW Rhodamine 6G dye laser with a new pumping source. A stable CW mode-locked Nd:YAG laser is externally frequency doubled using a temperature tuned Barium-Sodium-Niobate crystal ($Ba_2NaNb_5O_{15}$) and the green $\lambda = 532$ nm light serves as the pump. Using this method, dye laser pulses shorter than 2 psec are consistently observed.

The experimental setup is as shown in Fig. 24. A stable 8 W Nd:YAG laser was used with a pulsewidth FWHM of 50 psec or less. The infrared beam was focused into a temperature stabilized Barium-Sodium-Niobate frequency doubling crystal. $Ba_2NaNb_5O_{15}$ was chosen because of its high nonlinear coefficient and low absorption at both the fundamental and doubled wavelengths. This crystal can be 90° cut which, even in the focusing condition, allows generation of an undistorted second harmonic beam profile essential for optimum dye laser pumping.
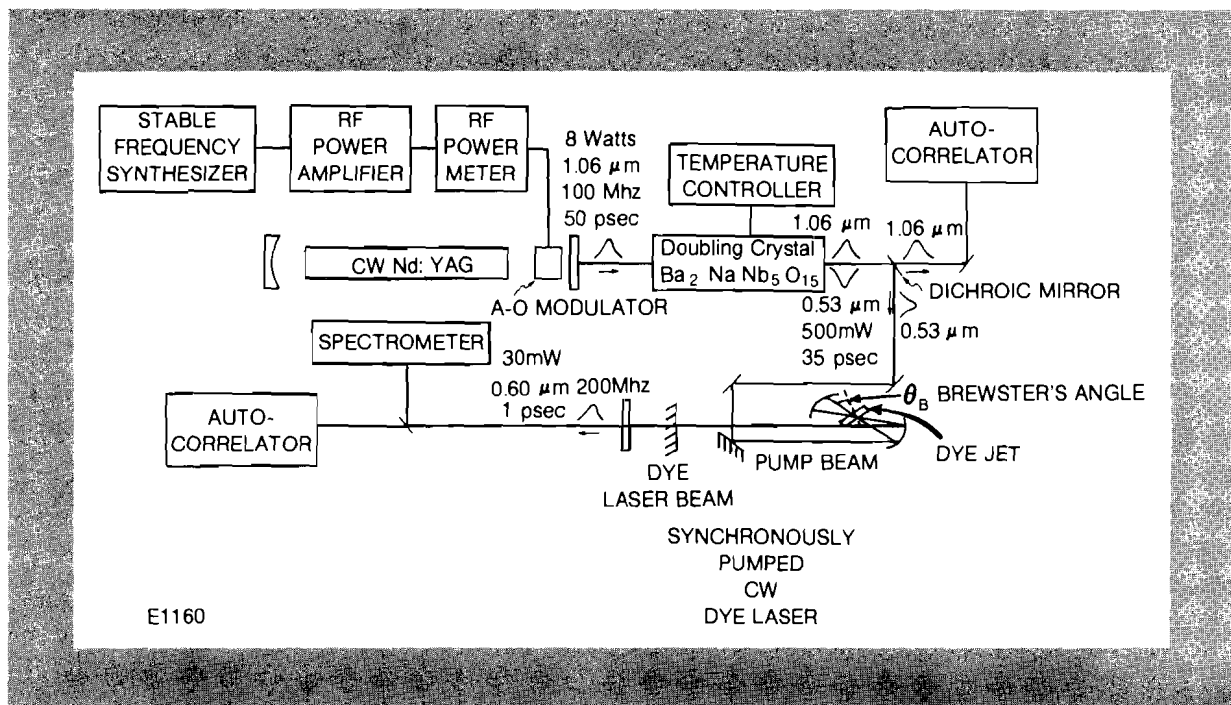
Fig. 24
Experimental setup of the synchro-
nously pumped dye laser. A stable CW
mode-locked Nd:YAG laser is externally
frequency doubled using a temperature
tuned Barium-Sodium-Niobate crystal
and the green light is used to pump a
dye laser. Dye laser pulses shorter
than 2 psec have consistently been
observed using this technique.

Pulsewidths consistently shorter than 2 psec have been achieved
without active stabilization. The output amplitude and pulsewidth
jitter of the dye laser is, as expected, strongly related to the
stability of the Nd:YAG. A slight amplitude instability of the
Nd:YAG is amplified because of the cumulative effect of the
frequency doubling and dye laser running at threshold. Subpico-
second pulses should be reliably achieved with the addition of
an active feedback stabilization system.

The benefits of using a frequency doubled Nd:YAG laser
instead of an argon-ion laser to pump a subpicosecond dye laser
are numerous. The pulsewidth of the doubled Nd:YAG can be
made to be shorter than the argon, and the reduced cost, lead
time, and installation of a lamp compared to an argon tube are
both considerable assets. Also, this system has the potential
advantage of being more suitable for short pulse amplification.
So far the amplification of short pulses from synchronously
pumped or passively mode-locked lasers has been achieved by
using a Q-switched laser electronically synchronized with the
short pulse laser.[6] The inherent jitter of a few nsec between the
two lasers leads to important amplitude instability when gain of
the order of 10^6 is contemplated.

In our scheme, part of the Nd:YAG can be used to seed a large
aperture regenerative amplifier. By synchronously pumping a
series of dye amplifiers with the frequency doubled output of the
regenerative amplifier, high conversion efficiencies in amplifying
the dye pulses can be achieved because ASE can be partially
defeated.

REFERENCES

1. J. M. Harris, R. W. Chrisman, and F. E. Lytle; *Appl. Phys. Lett.* **26,** 16 (1975).
2. J. P. Heritage and R. K. Jain; *Appl. Phys. Lett.* **32,** 101 (1978).
3. I. S. Ruddock and D. J. Bradley; *Appl. Phys. Lett.* **29,** 296 (1976).
4. D. J. Bradley; *Ultra Short Light Pulses,* S. L. Shapiro ed. (Springer, Berlin 1977), Chap. 2.
5. J. P. Ryan, L. S. Goldberg and D. J. Bradley; *Opt. Comm.* **27,** 127 (1978).
6. M. M. Salour, *Opt. Comm.* **22,** 202 (1977).

Section 5
NATIONAL LASER USERS
FACILITY NEWS

In the last quarter further users have been notified that their proposals have been funded by the Nevada office of DOE. These include: G. Dahlbacka (Physics International); B. Yaakobi (University of Rochester) with A. Burek (National Bureau of Standards); and G. Miley (University of Illinois). A preliminary shot, using the GDL laser system, was obtained for Larry Knight of Brigham Young University. A synthetic multilayer crystal was used to diffract x-rays from an irradiated target. A good quality spectrum was observed in the region of 1 KeV.

New proposals for user experiments have been received from H. Epstein (Battelle Memorial Institute), R. Lysiak (Texas Christian University), and D. Hon (Hughes Research Laboratories). A booth advertising the NLUF was displayed at the November meeting of the Plasma Physics Division of the American Physical Society in San Diego. This attracted attention and led to useful discussions with potential users.

Due to re-assignment of responsibilities at the Laboratory for Laser Energetics, Dr. Thomas Bristow has become the manager of the National Laser Users Facility, effective February 1, 1981. He reports to the Acting Director of LLE, Dr. Jay Eastman. Proposals and inquiries should be sent to Dr. Bristow. He can be contacted at (716) 275-2074 or FTS 430-2074.

PUBLICATIONS AND CONFERENCE PRESENTATIONS

Publications

R. S. Craxton, "Theory of High Efficiency Third Harmonic Generation of High-Power Nd:Glass Laser Radiation," *Opt. Comm.* **34**, 474-478 (1980).

W. Seka, S. Jacobs, J. Rizzo, R. Boni, and R. S. Craxton, "Demonstration of High Efficiency Third Harmonic Conversion of High Power Nd:Glass Laser Radiation," *Opt. Comm.* **34**, 469-473 (1980).

M. Stavola, M. Sceats, and G. Mourou "Picosecond Switching of a Multi-Kilovolt DC Bias With Laser-Activated Silicon at Low Temperature," *Opt. Comm.* **34**, 409-412 (1980).

M. Stavola, G. Mourou, and W. Knox, "Picosecond Time Delay Fluorimetry Using a Jitter-Free Streak Camera," *Opt. Comm.* **34**, 404-408 (1980).

J. Eastman, "The Scanning Fizeau Interferometer: An Automated Instrument For Characterizing Optical Surfaces," *Opt. Eng.* **19**, 810-814 (1980).

J. Kelly, D. Brown and K. Teegarden, "Time-Resolved Spectroscopy of Large Bore Xe Flashlamps For Use In Large Aperture Amplifiers," *App. Opt.* **19**, 3817-3823 (1980).

J. Hoose, "White Light AC Interferometry for Multiple Laser Path Length Equilization," *Opt. Eng.* **19**, 825-827 (1980).

K. Tanaka and L. Goldman, "Observations of Brillouin Sidescatter in Laser-Produced Plasmas," *Phys. Rev. Let.* **45**, 1558-1561 (1980).

B. Yaakobi, H. Deckman, P. Bourke, S. Letzring, and J. Soures, "X-Ray Absorption Fine-Structure Measurement Using a Laser-Compressed Target as a Source," *App. Phys. Let.* **37**, 767-769 (1980).

Forthcoming Publications

D. Berwald, and J. Maniscalco, "Laser Fusion Breeder Fueled Electricity Generation System," submitted to *Nuclear Technology.*

D. Berwald, and J. Maniscalco, "An Economics Method for Symbiotic Fusion-Fission Electricity," submitted *Nuclear Technology.*

W. Knox, W. Friedman, and G. Mourou, "A Simple Silicon Switch-Driven Psec Streak Camera," accepted by *Applied Physics Letters.*

R. S. Craxton and R. McCrory, "Two-Dimensional Calculations of Non-Spherical Laser Fusion Implosions," submitted to *Nuclear Fusion.*

C. Harrison, D. Turner, J. Wilson, M. DeWyngaert, and D. Hinkle, "Laser Cross-Linking of RNA Polymerase and DNA," submitted to the *Journal of the American Chemical Society.*

S. Skupsky, and S. Kacenjar, "Measuring Fuel ρR for Inertial Fusion Experiments Using Neutron Elastic-Scattering Reactions," accepted by the *Journal of Applied Physics.*

T. Dewandre, J. Albritton and E. Williams, "Fast-Ion Production by Suprathermal Electrons in Laser Fusion Plasmas," accepted by *Physics of Fluids.*

M. True, J. Albritton, and E. Williams, "Doppler Shift of Laser Light Reflected from Expanding Plasmas," accepted by *Physics of Fluids.*

R. McCrory, L. Montierth, R. Morse and C. Verdon, "Nonlinear Evolution of Ablation-Driven Rayleigh-Taylor Instability," submitted to *Physical Review Letters.*

R. McCrory. L. Montierth, R. Morse and C. Verdon, "Taylor Instability in Fusion Targets," submitted to *Laser Interactions and Relative Plasma Phenomena,* Vol. V. Plenum Press.

J. Soures, T. Bristow, H. Deckman, J. Delettrez, A. Entenberg, W. Friedman, J. Forsyth, Y. Gazit, G. Halpern, F. Kalk, R. McCrory, D. Peiffer, J. Rizzo, S. Skupsky, E. Thorsos, B. Yaakobi and T. Yamanaka, "A Review of High Density Laser-Driven Implosion Experiments at the Laboratory for Laser Energetics," submitted to *Laser Interactions and Relative Phenomena,* Vol. V. Plenum Press.

G. Mourou, C.V. Stancampiano, and D. Blumenthal, "Picosecond Microwave Pulse Generation," submitted to *Applied Physics Letters.*

T. Nordlund and W. Knox, "Lifetime of Fluorescence From Light-Harvesting Chlorophyll a/b Proteins: Excitation Intensity Dependence," submitted to *Biophysical Journal.*

G. Harvey, G. Mourou and C. Gabel, "Synchronization of a Mode-Locked Nd:YAG-Argon-Ion Laser System," accepted by *Optics Communications*.

J. Kelly, D. Brown, J. Abate and K. Teegarden, "A Dynamic Pumping Model for Amplifier Performance Predictions," submitted to *Applied Optics*.

D. Brown, J. Abate, L. Lund and J. Waldbillig, "Passively-Switched Double-Pass Active Mirror System," submitted to *Applied Optics*.

J. Abate, L. Lund, D. Brown, S. Jacobs, S. Refermat, J. Kelly, M. Gavin, J. Waldbillig and O. Lewis, "Active Mirror: A Large Aperture, Medium-Repetition Rate Nd:Glass Amplifier," accepted by Applied Optics.

R. Turner and L. Goldman, "Evidence for Multiple Brillouin Modes in Laser-Plasma Backscatter Experiments," accepted by *Physics of Fluids*.

Conference Presentations

W. Seka, "Progress in Laser Fusion Research," presented at the Fall Meeting of the Austrian Physical Society, September 1980.

H. Deckman, J. Dunsmuir and G. Halpern, "A Drill, Fill and Plug Technique for Fabricating Laser Fusion Targets," presented at the American Vacuum Society Meeting, October 1980.

H. Deckman, "Micromachining Applications for ICF Target Fabrication," presented at the American Vacuum Society Meeting, October 1980.

I. Goldstein and F. Kalk, "Oxygen Plasma Etching of Thick Polymer Layers," presented at the American Vacuum Society Meeting, October 1980.

I. Goldstein and J. Varon, "DC Deposition Source Dependence of the Surface Morphology of Copper Sputter-Coated Laser Fusion Targets," presented at the American Vacuum Society Meeting, October 1980.

L. Forsley, "A Relational Methodology for Process Control and Data Acquisition Using FORTH and CAMAC with DEC PDP 11 Architecture," presented at the Fall Decus U.S. Symposium, November 1980.

R. Bingham and C. Lashmore-Davies, "Filamentation Re-Visited," presented at the Annual Meeting of the APS Division of Plasma Physics, November 1980.

T. Bristow, J. Boles, J. Delettrez, A. Entenberg, J. Forsyth, S. Kumpan, S. Letzring, M. Lubin, R. McCrory, M. Richardson and J. Soures, "Initial Experiments on OMEGA," presented at the Annual Meeting of the APS Division of Plasma Physics, November 1980.

R S. Craxton and R. McCrory, "Two-Dimensional Calculations of the Interaction of UV Laser Light with Low-Z Targets," presented at the Annual Meeting of the APS Division of Plasma Physics, November 1980.

J. Delettrez, T. Bristow, A. Entenberg, J. Soures and E. Thorsos, "Analysis of Exploding-Pusher Implosion Experiments," presented at the Annual Meeting of the APS Division of Plasma Physics, November 1980.

A. Entenberg, T. Bristow, J. Delettrez, Y. Gazit and J. Soures, "Ion Temperature Dependence on Specific Absorbed Energy in Six-Beam Symmetrical Implosion Experiments," presented at the Annual Meeting of the APS Division of Plasma Physics, November 1980.

R. Epstein, S. Skupsky and R. McCrory, "Improvements in the Treatment of Radiative Transfer in One-Dimensional Laser Fusion Simulations," presented at the Annual Meeting of the APS Division of Plasma Physics, November 1980.

W. Friedman, S. Letzring, E. Thorsos and W. Seka, "Processing and Interpretation of X-Ray Streak Camera Images," presented at the Annual Meeting of the APS Division of Plasma Physics, November, 1980.

L. Goldman and S. Sarraf, "Effect of Prepulse on Non-Thermal (> 10 KeV/Z) Ions in Laser Produced Plasma," presented at the Annual Meeting of the APS Division of Plasma Physics, November 1980.

S. Kacenjar, S. Skupsky, L. Goldman and A. Entenberg, "Measuring Fuel ρR in Laser Fusion Using CR-39 Solid State Track Detectors," presented at the Annual Meeting of the APS Division of Plasma Physics, November 1980.

F. Kalk and J. Forsyth, "Effects of Nonlinearities on Image Fidelity in Zone Plate Coded Imaging," presented at the Annual Meeting of the APS Division of Plasma Physics, November 1980.

S. Letzring, E. Thorsos, W. Friedman, P. Bourke and A. Wilson, "X-Ray Imaging Measurements of Illumination Uniformity and Implosion Symmetry on ZETA," presented at the Annual Meeting of the APS Division of Plasma Physics, November 1980.

J. McAdoo and L. Goldman, "Dependence of MeV X-Rays on Laser Intensity in Laser Fusion Experiments," presented at the Annual Meeting of the APS Division of Plasma Physics, November 1980.

R. McCrory, R. Morse and C. Verdon, "Saturation of Ablation-Driven Rayleigh-Taylor Instability," presented at the Annual Meeting of the APS Division of Plasma Physics, November 1980.

B. Nicholson, W. Seka, L. Forsley and D. Blumenthal, "High Power UV (0.351 μm) Laser-Plasma Absorption Studies," presented at the Annual Meeting of the APS Division of Plasma Physics, November 1980.

S. Sarraf, E. Williams and L. Goldman, "Ion-Ion Two-Stream Instability in Multispecies Streaming Plasma," presented at the Annual Meeting of the APS Division of Plasma Physics, November 1980.

W. Seka, T. Boehly, R. S. Craxton, L. Forsley, L. Goldman, S. Jacobs, R. Keck, B. Nicholson, R. McCrory, M. Richardson, J.

Rizzo, J. Soures and K. Tanaka, "Preliminary Results of Laser-Matter Interaction Experiments at 0.35 μm," presented at the Annual Meeting of the APS Division of Plasma Physics, November 1980.

R. Short and E. Williams, "Enhanced Specular Reflection From a Laser Plasma Source," presented at the Annual Meeting of the APS Division of Plasma Physics, November 1980.

S. Skupsky, B. Yaakobi and C. Hooper, "Simulation of X-Ray Spectra From the Implosion of Argon Filled Microballoons," presented at the Annual Meeting of the APS Division of Plasma Physics, November 1980.

K. Tanka and L. Goldman, "Observations of Brillouin Side-Scatter in Laser Produced Plasma," presented at the Annual Meeting of the APS Division of Plasma Physics, November 1980.

E. Thorsos, W. Seka, T. Bristow, A. Entenberg, W. Friedman, S. Letzring, J. Soures, J. Delettrez and R. McCrory, "Experimental Scaling Laws of Six-Beam Intermediate Density Microballoon Implosions," presented at the Annual Meeting of the APS Division of Plasma Physics, November 1980.

C. Verdon, R. McCrory and R. Morse, "Nonlinear Development and Saturation of Ablation-Driven Rayleigh-Taylor Instability in Thin Shells," presented at the Annual Meeting of the APS Division of Plasma Physics, November 1980.

E. Williams, M. True and J. Albritton, "Coupling of Hot Electrons to Laser Fusion Targets II," presented at the Annual Meeting of the APS Division of Plasma Physics, November 1980.

B. Yaakobi, S. Skupsky, W. Friedman, R. McCrory, H. Deckman, P. Bourke, S. Letzring and J. Soures, "High Density and Compression Ratio Measured Spectroscopically in Radiationally Cooled Targets," presented at the Annual Meeting of the APS Division of Plasma Physics, November 1980.